



Published in final edited form as:

*Cancer Discov.* 2020 September ; 10(9): 1388–1409. doi:10.1158/2159-8290.CD-19-1436.

## Posttranslational regulation of the exon skipping machinery controls aberrant splicing in leukemia

Yalu Zhou<sup>1,2</sup>, Cuijuan Han<sup>1,2</sup>, Eric Wang<sup>3</sup>, Adam H. Lorch<sup>1,2</sup>, Valentina Serafin<sup>4</sup>, Byoung-Kyu Cho<sup>5</sup>, Blanca T. Gutierrez Diaz<sup>1,2</sup>, Julien Calvo<sup>6,7</sup>, Celestia Fang<sup>1,2,8</sup>, Alireza Khodadadi-Jamayran<sup>9</sup>, Tommaso Tabaglio<sup>10,11</sup>, Christian Marier<sup>12</sup>, Anna Kuchmiy<sup>13,14</sup>, Limin Sun<sup>1,2</sup>, George Yacu<sup>1,2</sup>, Szymon K. Filip<sup>5</sup>, Qi Jin<sup>1,2</sup>, Yoh-hei Takahashi<sup>1,2</sup>, David R. Amici<sup>1,2,8</sup>, Emily J. Rendleman<sup>1,2</sup>, Radhika Rawat<sup>1,2,8</sup>, Silvia Bresolin<sup>4</sup>, Maddalena Paganin<sup>4</sup>, Cheng Zhang<sup>15</sup>, Hu Li<sup>15</sup>, Irawati Kandela<sup>16</sup>, Yuliya Politanska<sup>17</sup>, Hiam Abdala-Valencia<sup>17</sup>, Marc L. Mendillo<sup>1,2</sup>, Ping Zhu<sup>18</sup>, Bruno Palhais<sup>13,19</sup>, Pieter Van Vlierberghe<sup>13,19</sup>, Tom Taghon<sup>13,14,20</sup>, Iannis Aifantis<sup>3</sup>, Young Ah Goo<sup>1,5</sup>, Ernesto Guccione<sup>21,22</sup>, Adriana Heguy<sup>3,12</sup>, Aristotelis Tsirigos<sup>3,9</sup>, Keng Boon Wee<sup>9,10</sup>, Rama K. Mishra<sup>1,23</sup>, Françoise Pflumio<sup>6,7</sup>, Benedetta Accordi<sup>4</sup>, Giuseppe Basso<sup>4</sup>, Panagiotis Ntziachristos<sup>1,2,24,\*</sup>

<sup>1</sup>Department of Biochemistry and Molecular Genetics, Northwestern University, Chicago, IL, USA

<sup>2</sup>Simpson Querrey Center for Epigenetics, Northwestern University Feinberg School of Medicine, Chicago, IL, USA

<sup>3</sup>Department of Pathology and Laura & Isaac Perlmutter Cancer Center, NYU School of Medicine, New York, NY, USA

<sup>4</sup>Oncohematology Laboratory, Department of Women's and Children's Health, University of Padova, Padova, Italy

\*Correspondence should be addressed to: Panagiotis Ntziachristos, Assistant Professor, Department of Biochemistry and Molecular Genetics, Feinberg School of Medicine, Simpson Querrey Biomedical Research Building, 7th floor, 7-304, 303 East Superior Street, Chicago, IL 60611, pntziachr@gmail.com, Office phone: 312.503.5225, Cell phone: 347.703.0048, Fax: 312.503.4081, Website: [Ntziachristoslab.com](http://Ntziachristoslab.com).

### Author Contributions

P.N. designed the study, performed and interpreted most of the experiments, and wrote the manuscript. Y.Z. designed the study, performed and interpreted experiments; directed the bioinformatics analysis; and wrote the manuscript. C.H. designed and executed experiments, interpreted the results and contributed to the writing of the manuscript. B.T.G.D. and A.H.L. designed and performed experiments. G.Y., C.F., Q.J., R.R., and Y.T. helped with execution of experiments, and contributed ideas. H.A.-V., Y.P. and E.J.R. performed or helped with the execution of next-generation sequencing. H.L. and C.Z. helped with bioinformatics analysis. I.K. performed and analyzed the xenograft studies. B.A., V.S., M.P., G.B., and S.B. performed and analyzed the RPPA, associated gene expression studies, and targeted sequencing of splicing factors, and provided patient samples. A.K. and T.T. isolated, characterized and processed thymic samples. B.-K.C., S.K.F. and Y.A.G. performed the mass spectrometry experiment and analysis. R.M. performed in silico modeling of PSMG1-201 and 202 structures. P.Z. provided the H3B-8800 compound and advised on the use of it. P.V.V. and B.P. provided human patient samples and helped with ideas and the writing of the manuscript. A.T. and A. K.-J. helped with analysis of splicing data. D.K.B., T.T. and E.G. helped with the design of antisense oligos for PSMG1 exon skipping. D.R.A. and M.L.M. helped with the analysis, interpretation, and integration of the DepMap data. E.W. and I.A. designed, executed, and analyzed the RBP CRISPR/Cas9 screen experiment and provided feedback on the manuscript. J.C. and P.F. designed, executed and interpreted drug treatments and associated phenotypes in patient samples.

**Competing Interests:** Ping Zhu is an employee at H3 Biomedicine. The other authors have no conflicts of interest.

### Data availability

The raw files for our proteomics studies are deposited in MassIVE (accession: *MSV000084383*) <https://massive.ucsd.edu/ProteoSAFe/static/massive.jsp>

The login information for reviewers at MassIVE is:

Username: cbk562

Password: 3125033711

The raw files for our next-generation sequencing data have been deposited in Gene Expression Omnibus (GEO, *GSE139622*).

- <sup>5</sup>Proteomics Center of Excellence, Northwestern University, Evanston, IL, USA
- <sup>6</sup>Team Niche and Cancer in hematopoiesis, CEA, Fontenay-aux-Roses, France
- <sup>7</sup>Laboratory of Hematopoietic Stem Cells and Leukemia/Service Stem Cells and Radiation /IRCM/JACOB/DRF, CEA, Fontenay-aux-Roses, France
- <sup>8</sup>Medical Scientist Training Program, Northwestern University Feinberg School of Medicine, Chicago, IL, USA
- <sup>9</sup>Applied Bioinformatics Laboratories, Office of Science and Research, New York University School of Medicine, New York, NY, USA
- <sup>10</sup>Institute of Molecular and Cell Biology, Agency for Science, Technology and Research, Singapore
- <sup>11</sup>Department of Biochemistry, Yong Loo Lin School of Medicine, National University of Singapore, Singapore
- <sup>12</sup>Genome Technology Center, New York University School of Medicine, New York, United States
- <sup>13</sup>Cancer Research Institute Ghent (CRIG), Ghent, Belgium
- <sup>14</sup>Department of Diagnostic Sciences, Ghent University, Ghent, Belgium
- <sup>15</sup>Department of Molecular Pharmacology and Experimental Therapeutics, Mayo Clinic, Rochester, MN, USA
- <sup>16</sup>Center for Developmental Therapeutics, Northwestern University, Evanston, IL, USA
- <sup>17</sup>Department of Medicine, Northwestern University Feinberg School of Medicine, Chicago, IL, USA
- <sup>18</sup>H3 Biomedicine, Inc., Cambridge, MA, USA
- <sup>19</sup>Department of Biomolecular Medicine, Ghent University, Ghent, Belgium
- <sup>20</sup>Faculty of Medicine and Health Sciences, Ghent University, Ghent, Belgium
- <sup>21</sup>Department of Oncological Sciences and Tisch Cancer Institute, Icahn School of Medicine at Mount Sinai
- <sup>22</sup>Department of Pharmacological Sciences and Mount Sinai Center for Therapeutics Discovery, Icahn School of Medicine at Mount Sinai, New York, NY, USA
- <sup>23</sup>Center for Molecular Innovation and Drug Discovery, Northwestern University, Chicago, IL, USA
- <sup>24</sup>Robert H. Lurie Comprehensive Cancer Center, Northwestern University, Chicago, IL, USA

## Abstract

Splicing alterations are common in disease, such as cancer, where mutations in splicing factor genes are frequently responsible for aberrant splicing. Here we present an alternative mechanism for splicing regulation in T cell acute lymphoblastic leukemia (T-ALL), that involves posttranslational stabilization of the splicing machinery via deubiquitination. We demonstrate there are extensive exon skipping changes in disease affecting proteasomal subunits, cell cycle

regulators, and the RNA machinery. We present that the serine/arginine-rich splicing factors (SRSF), controlling exon skipping, are critical for leukemia cell survival. The ubiquitin-specific peptidase 7 (USP7) regulates SRSF6 protein levels via active deubiquitination and USP7 inhibition alters the exon skipping pattern and blocks T-ALL growth. The splicing inhibitor H3B-8800 affects splicing of proteasomal transcripts and proteasome activity and acts synergistically with proteasome inhibitors in inhibiting T-ALL growth. Our study provides the proof-of-principle for regulation of splicing factors via deubiquitination and suggests new therapeutic modalities in T-ALL.

## INTRODUCTION

Alternative splicing is a critical mechanism of post-transcriptional regulation that is mediated by the ribonucleoprotein complex commonly known as the spliceosome. It is estimated that more than 90% of transcripts from multiexonic protein-coding transcripts could be alternatively spliced in a tissue- or developmental stage-specific manner, under stress or in disease<sup>1</sup>. While the average human gene produces three or more alternatively spliced mRNA isoforms, malignant cells produce a significant surplus of splice variants. These atypical splice variants appear to be products of mis-splicing that in many cases are secondary to either mutations in splicing factors or dysregulation of their expression. The prevalence of these anomalies in the splicing machinery is elevated in certain types of hematologic malignancies, and provides a unique opportunity for therapeutic targeting<sup>2-4</sup>.

The splicing machinery is frequently mutated in the early stages of many types of cancer, such as myelodysplastic syndromes or chronic lymphocytic leukemia, demonstrating the importance of this pathway for cellular function<sup>2-14</sup>. Aberrant splicing is mostly attributed to genetic alterations affecting the splicing factor genes. These mutations occur most commonly in *SF3B1* (splicing factor 3b subunit 1), *SRSF2* (serine/arginine-rich splicing factor 2), *ZRSR2* (zinc finger RNA binding motif and serine/arginine rich 2), and *U2AF1* (U2 small nuclear RNA auxiliary factor 1) and in a mutually exclusive fashion, as mutations in more than one factor are lethal for tumor and normal cells alike<sup>15</sup>. Additionally, mutations affecting RNAs that are part of the spliceosome were recently identified<sup>16</sup>. However, splicing abnormalities found in cancer are not always associated with mutations in these or related genes. Instead, they may arise from aberrant expression of splicing factors<sup>17-26</sup>. Certain serine/arginine-rich (SR) splicing factor proteins are overexpressed in human cancers, notably SRSF1<sup>17-20,26</sup>, SRSF6<sup>17,21,22</sup>, and SRSF3<sup>23-25</sup>. Part of this activation might be due to gene amplification as well as transcriptional regulation, mainly through MYC. Expression-related variations in splicing are mostly observed in solid tumors of adult origin, suggesting a potential explanation for differences in splicing biology between solid and blood-based cancers.

Acute lymphoblastic leukemia (ALL) is an aggressive pediatric and adult type of leukemia of T- and B-cell origin translating to approximately 3,100 children and adolescents are diagnosed with the disease each year in the United States. T-cell ALL (T-ALL) is driven by the hyperactivation of pathways such as NOTCH1<sup>27-32</sup> and the incidence of this disease subtype is increasing<sup>33</sup>. One-fifth of pediatric patients and more than 50% of adult patients

with T-ALL do not achieve a complete remission or relapse after consolidated chemotherapy, making resistance to therapy the most substantial challenge in disease treatment<sup>31,34,35</sup>. T-ALL is an epigenetic disease presenting with deregulation of epigenetic enzymes. As many T-ALL oncogenes are transcription factors, disease initiation and progression are coordinated via epigenetic regulators in the cell nucleus. Work by our lab and others have described the major epigenetic players in this disease<sup>27,28,36–47</sup>. However, the design of treatment strategies based on direct inhibitors of these proteins has been challenging, as oncogenes such as NOTCH1 are broadly involved in physiologic processes. Furthermore, there are very few documented mutations affecting splicing factors in T-ALL<sup>48</sup>, and the splicing landscape in T-ALL is relatively poorly characterized. Thus, as of this writing, we lack evidence-based strategies for treating cancers like T-ALL that have no or very few splicing factor mutations. In addition, mechanisms of resistance in T-ALL remain poorly characterized due to the absence of appropriate leukemia models and needed technologies.

Although we and others have previously demonstrated the role of epigenetic factors and oncogenic long non-coding RNAs in T-ALL<sup>41–43</sup>, the role of aberrant splicing and mechanisms of abnormal post-translational regulation of the splicing machinery in T-ALL progression have been relatively uncharacterized. In this study, we sought to characterize splicing alterations in T-ALL, potential mechanisms regulating aberrant splicing, and their implications for T-ALL biology.

## RESULTS

### T-ALL is characterized by significant splicing changes compared to physiological T cells

To characterize the splicing landscape in different types of human peripheral CD3<sup>+</sup> (CD4<sup>+</sup>/CD8<sup>+</sup>) T cells, in comparison to three T cell leukemia patients, we performed paired-end sequencing of the transcriptome to cover the splicing junctions. To study any T cell subtype-specific and differentiation stage-specific phenomena we also included a T cell subtype, CD4<sup>+</sup> T cells, and undifferentiated fast-proliferating thymocytes. Initial expression analysis of normal and tumor samples using edgeR<sup>49</sup> showed a significant up-regulation of oncogenic targets in T-ALL, including NOTCH1 targets, as well as cell cycle regulators, in agreement with previous findings in human and mouse contexts of T-ALL<sup>41</sup> (Fig 1A and Supplementary Fig. 1A–D, Supplementary Tables 1–3). We then used rMATS<sup>50</sup>, an established method for quantitative analysis of differential splicing phenomena, to cluster splicing changes between peripheral CD3<sup>+</sup> T cells and T-ALL, in five distinct categories: exon skipping, intron retention, mutually exclusive exons, and usage of alternative 3' or alternative 5' splice sites (Fig. 1B and Supplementary Fig. 1E). We observed changes for each of these splicing categories between the two cell populations, with the most extensive splicing changes affecting skipped exons and retained introns (Fig. 1B, C and Supplementary Figs. 1E, 2A, B). Overall, there was a significant increase of exon skipping events in T-ALL cells compared to normal T cells (see red bar representing excluded exons, Fig. 1C). An alternative analysis quantifying exon inclusion levels and comparison of normal T cell subsets with T-ALL patients showed there are more exon inclusion phenomena in T cells compared to T-ALL (Supplementary Fig. 2C). In conclusion, T cell

cancers present with a higher number of skipped exon phenomena compared to physiological T cells.

By performing a transcript-based analysis, we identified a total of 1,583 alternatively spliced transcripts in T-ALL compared to all three physiological T cell subsets (Fig. 1D, false discovery rate (*FDR*)<0.05). We noticed significant changes in spliceosome and RNA transport-related transcripts (Fig. 1E and Supplementary Table 4). We also report extensive changes in proteasome, apoptosis, and cell cycle-related transcripts (Fig. 1E and Supplementary Table 4). More comprehensive splicing analysis in T cell subsets showed extensive similarities with each other and differences when compared to T-ALL (Supplementary Fig. 2D). We further compared the different T cell subsets to show that splicing phenomena reflect their developmental stages; differentiated CD4<sup>+</sup> cells present 1668 alternatively regulated splicing events compared to CD3<sup>+</sup> T cells and 3129 alternatively regulated splicing events compared to undifferentiated thymocytes (Supplementary Fig. 2E). These differences in splicing between T cell subtypes potentially recapitulate biological characteristics<sup>51</sup> (Supplementary Fig. 2F). For instance, faster proliferation is a major difference between T cell progenitors in the thymus and terminally differentiated T cells. Indeed, gene ontology analysis of thymocyte-specific splicing phenomena showed that cell cycle transcripts are differentially spliced between differentiated CD3<sup>+</sup> and CD4<sup>+</sup> cells and thymocytes (Supplementary Fig. 2G and Supplementary Table 5). Our findings suggest that the splicing landscape recapitulates lineage- or development-related biological characteristics.

We then performed further filtering based on the ‘percent spliced in’ (*PSI*, or splicing inclusion level, 0 (0%) to 1 (100%))<sup>1</sup> value changes between T cell subsets and T-ALL, after normalizing all transcripts belonging to a specific isoform or alternatively spliced sequence of interest relative to all transcripts of the gene. In this case, we consider significant only changes bigger than 10% or *PSI*>0.1. Focusing on transcript categories enriched in our enrichment analysis, we identified alternative splicing events affecting RNA transportation (e.g. NUP85), proteasomal-related transcripts (e.g. *PSMG1*, *PSMB9*, *PSMD4*, *PSMC3IP*), cell cycle transcripts (*CCND3*), epigenetic enzymes (*CREBBP* or *CBP*) and apoptotic factors (*BCL2L11*) (Fig. 1F (for CD3<sup>+</sup> T cells vs. T-ALL)). Spliceosome components were also enriched in the differentially spliced transcripts, with a particular enrichment for serine/arginine-rich splicing factor (SRSF) transcript family (e.g. *SRSF2*, *SRSF3*, *SRSF6*, *SRSF7*). We noticed a similar enrichment in alternatively spliced spliceosome, proteasome and RNA biology-related transcripts under more stringent conditions as well (*PSI*> 0.2, Supplementary Fig. 3A, B). We then sought out to confirm splicing changes affecting exon skipping and intron retention in SRSF factors (Supplementary Fig. 3C). SRSF levels are controlled via a process called nonsense mediated decay (NMD), where transcripts containing a premature termination codon are degraded by the cellular machinery coordinated via binding of the regulator of nonsense transcripts 1 (UPF1). The *SRSF6* NMD allele contains exon 3 (poison exon) that, in turn, contains a termination codon<sup>52,53</sup>. We detect exon 3 in T cell samples, and we show it is skipped in T-ALL (Supplementary Fig. 3C, D). Additionally, silencing of *UPF1* in leukemia cells led to a slight but significant increase of the *SRSF6* NMD allele (Supplementary Fig. 3E–G). These results provide evidence for regulation of the *SRSF6* transcript levels via NMD in T cells. An unbiased de

novo motif analysis using the rMAPS2 Motif Map<sup>54</sup> using exon skipping-associated areas between CD3<sup>+</sup> T cells and T-ALL, identified the previously characterized SRSF6-bound sequence<sup>22</sup> as the top motif in the exon-intron junction upstream of the skipped exon (*in purple*, Fig. 1G and Supplementary Table 6), suggesting a potential role for SRSF6 in controlling exon skipping in T-ALL.

We next sought to map splicing changes in T-ALL cases that do not respond to chemotherapy or that relapse (“high-risk” (HR)), which represent the main therapeutic unmet need in T-ALL. This risk of disease relapse is determined based on the detection (HR) or not (“non-high-risk” (NHR) disease) of residual cancer cells on day 35 from initiation of chemotherapy treatment. We sequenced 4 HR and 10 NHR diagnostic samples to validate splicing changes in T-ALL. Using this new patient group (validation cohort) we initially confirmed that there are more exon skipping events in T-ALL cells compared to CD3<sup>+</sup> T cells (Supplementary Fig. 4A, B). We show that similar to what we presented in Supplementary Fig. 2C, analysis of this larger patient set shows that there is a significantly higher number of exon inclusion phenomena (exon inclusion levels, EIL) in CD3<sup>+</sup> T cells compared to T-ALL (Supplementary Fig. 4A), and inversely an increased number of exon skipping phenomena in T-ALL affecting proteasome transcripts, as well as cell cycle regulator- and epigenetic enzyme-related transcripts (Supplementary Fig. 4B). We next compared splicing changes in HR and NHR T-ALL patients, and saw a dramatic increase in exon skipping events and a decrease in mutually exclusive exon events in HR T-ALL compared to NHR (Supplementary Fig. 4C). Further transcript-based gene ontology analysis of the affected transcripts showed that alternative splicing phenomena are related to the chemotherapy resistance observed in HR cases, such as DNA damage response and DNA repair, as well as to spliceosome, the proteasome, cell cycle, and epigenetic regulators (Supplementary Fig. 4D and Supplementary Table 7). Exon skipping and mutually exclusive exon changes between T-ALL and T cells as well as between HR and NHR cases, and are a hallmark of altered function of SR splicing factor (SRSF) proteins<sup>18,22</sup>.

### Serine/arginine-rich splicing factor levels are critical for T-ALL cell survival

Driven by the extensive number of exon skipping events in T-ALL, we sought to characterize the importance of individual SRSF proteins in T-ALL in an unbiased manner. To this end, we analyzed CRISPR/Cas9 screen data from the Cancer Dependency Map project (*DepMap*, <https://depmap.org/portal/>) using 563 cell lines<sup>55</sup> from solid and blood-based tumors, including three T-ALL cell lines (SUPT1, PF382, HSB2, Supplementary Table 8). These data show that T-ALL cells are sensitive to SRSF deletion, in comparison to other cancer types (Fig. 1H and Supplementary Fig. 5A–K). Strikingly, T-ALL is the cancer type that is the most sensitive to *SRSF6* deletion (Fig. 1I). We further performed an in-house type II CRISPR system screen in JURKAT cells using a custom 2,900-single-guide RNAs (sgRNAs, ~6–8 per gene) library against 490 well-defined RBPs<sup>56–58</sup>, similar to previous studies<sup>59–61</sup>. In this negative selection screen, depletion of specific sgRNAs in the cell population were assessed over time<sup>58,62</sup>. Individual sgRNA read counts were evaluated by next-generation sequencing using genomic DNA from cells on day 4 and day 20 post-transduction of cells with viruses expressing the sgRNA library. For a given gene, we measured the average fold change of relative abundance of all sgRNAs targeting the gene on

day 4 and day 20. This negative selection screen revealed a strong enrichment for 60 RBPs including 7 SRSF factors (SRSF1, 2, 3, 6, 7, 10, and 11) in the depleted cell population (Supplementary Fig. 5L and Supplementary Table 9). To study the extent to which SRSF6 levels associate with disease prognosis in human T-ALL, we analyzed expression data for the SRSF factors, aside from SRSF8 which is expressed at very low levels in T-ALL, coupled to survival data from the pediatric cancer genome project (PECAN), to show that *SRSF6* and *SRSF1* are the only SRSF members whose high expression associates with unfavorable disease prognosis in T-ALL (Supplementary Fig. 6A–K). The aforementioned findings, reached via two independent CRISPR-based studies--the *DepMap* study and our CRISPR screen--as well as via patient survival data underline the importance of SRSF family members, and SRSF6 in particular, for acute leukemia survival.

### SRSF proteins are post-translationally regulated in T-ALL

As exon skipping and mutually exclusive exon phenomena could be a result of alterations in SRSF levels due to mutations, genetic amplification, transcriptional up-regulation or post-translational regulation<sup>3,4,22</sup>, we initially studied genetic alterations in *SRSFs* and selected splicing factor genes frequently altered in other types of cancer such as *SF3B1*, *U2AF1*, and *ZRSF2*, in CUTLL1 and JURKAT cell lines, as well as our cohort of diagnostic samples used in Fig. 1 and Supplementary Fig. 4. We performed targeted sequencing to identify that only JURKAT cells (SF3B1, Val1128Ile) and one patient sample (SRSF7, Asn177Tyr) exhibit mutations in the splicing machinery (Supplementary Table 10). Additionally, analysis of a pediatric cohort of 264 T-ALL patients from the pediatric cancer genome project (PECAN)<sup>48</sup>, as well as a cohort of adult T-ALL cases<sup>63</sup>, showed a small percentage of T-ALL cases with splicing factor mutations (Supplementary Fig. 7A, and B (left panel)), in contrast to other cancers such as chronic lymphocytic leukemia and myelodysplastic syndromes (CLL and MDS, Supplementary Fig. 7B, middle and right panel), which exhibit more frequent mutations in the splicing machinery<sup>2-4,11,13,64,65</sup>. This suggests there might be other ways the splicing could go awry in T-ALL, including transcriptional and post-translational regulation.

We then studied the transcriptional levels of SRSFs in the T-ALL transcriptome, using a previously published large T-ALL cohort<sup>66</sup> to demonstrate a significant increase of select *SRSF* transcripts, including SRSF6, in T-ALL compared to normal T cells (Supplementary Fig. 7C, D). It was previously shown that splicing components, including SRSF1, might be controlled by MYC<sup>18,19,67</sup> and that splicing inhibition might be a therapeutic approach in MYC-positive tumors<sup>68</sup>. Additionally, NOTCH1 has been shown to transcriptionally control the *SQHI* splicing factor in T-ALL<sup>69</sup>. Both NOTCH1 and MYC are major oncogenes in T-ALL and our group has previously shown that NOTCH1 recruits USP7 to chromatin to promote transcriptional activation of oncogenic targets<sup>70</sup>. Nevertheless, inhibition of NOTCH1 and MYC activity in human T-ALL cell line JURKAT using gamma secretase and bromodomain inhibitors, respectively, yielded very few changes in splicing factors in general, and no changes in SRSF6 levels (Supplementary Fig. 7E). These findings demonstrate that SRSFs might be regulated in alternative, both direct and indirect, ways in T-ALL.

Initially, assessment of protein levels for SRSF6 in T-ALL patient samples showed that it collectively exhibits a significantly higher expression in T-ALL (Fig. 2A, B), and also exhibits a significant positive correlation between SRSF6 and USP7 protein levels in T-ALL (Fig. 2C). To further study the relevance of SRSF6 protein levels and biology in human T-ALL patient samples, we performed an analysis of SRSF6 protein levels in T-ALL patient samples using reverse phase protein array (RPPA) with 14 HR and 31 NHR samples. There is a significant up-regulation of SRSF6 protein levels in aggressive HR vs. NHR leukemia (Fig. 2D). In contrast to protein levels, the mRNA levels of *SRSF6* are not different in aggressive disease (HR) cases compared to non-aggressive (standard- and low-risk) T-ALL or among the different T-ALL subsets (Supplementary Fig. 7F, G).

As our group recently characterized the major pro-oncogenic role of the deubiquitinase USP7 in T-ALL<sup>70,71</sup> we examined protein levels of SRSF6 in comparison to USP7 levels in this larger patient cohort of HR and NHR patients. Similar to Fig. 2C, we noticed that SRSF6 protein levels significantly correlate with USP7 levels (Fig. 2E). We then performed USP7 pull-down studies coupled to mass spectrometry analysis in JURKAT cells to characterize the USP7 interactome. We identified that USP7 interacts with select splicing factors, with SRSFs 3, 6, 7, and 10 being among the most enriched interactors (Fig. 2F and Supplementary Table 11). These findings suggest that USP7 might control protein stabilization of SRSF6 via deubiquitination. To study the extent to which USP7 controls the ubiquitination levels of SRSF6, we screened for ubiquitination changes in the human proteome. We treated JURKAT cells with vehicle or USP7 inhibitor P5091 over a period of 24 h followed by global pull-down of ubiquitinated lysine residues in lysine-glycine-glycine (KGG) moieties using equal input protein amounts of whole cell extracts (Fig. 2G). Mass spectrometry analysis generated a list of 393 differentially ubiquitinated proteins (Supplementary Table 12). Gene ontology analysis showed a significant enrichment in RNA binding proteins (Fig. 2H and Supplementary Table 13). To identify direct USP7 substrates in T-ALL, we assessed the convergence of the differentially ubiquitinated proteins upon treatment with P5091 with the USP7 interactome (see Fig. 2F) to identify 58 proteins as direct USP7 substrates (Supplementary Fig. 8A and Supplementary Table 13). Gene ontology analysis of the convergent set showed a significant enrichment of RNA binding proteins such as the RNA splicing machinery and RNA metabolizing enzymes, including SRSF6, which presents with increased ubiquitination levels upon P5091 treatment ( $n=25$ , Fig. 2I and Supplementary Fig. 8B). To further study USP7-mediated deubiquitination of SRSF6, we expressed Flag-SRSF6 in CUTLL1 cells, coupled to treatment with vehicle or P5091, to test for changes in SRSF6 ubiquitination upon inhibition of USP7. Our results demonstrate the increase of SRSF6 ubiquitination upon P5091 treatment (Fig. 2J). To assess the importance of the catalytic activity of USP7 for the regulation of SRSF6 ubiquitination, we expressed SRSF6 and ubiquitin in the presence of wild-type catalytically active as well as catalytically deficient USP7 (USP7 CD). We show that there is a significant decrease in SRSF6 ubiquitination upon wild-type USP7, but not upon USP7 CD, expression (Supplementary Fig. 8C). As SRSF factors can be controlled at the posttranslational level via neddylation<sup>72,73</sup>, we further tested whether SRSF6 can be neddylated. Our studies showed that SRSF6 is not neddylated, in contrast to SRSF3 which present with detectable levels of



neddylation in agreement with previous studies<sup>72,73</sup> (Supplementary Fig. 8D). These studies suggest a role of the USP7 deubiquitinase activity in controlling SRSF6 protein levels.

We further validated the interaction between endogenous USP7 and SRSF6 proteins in JURKAT and CUTLL1 T-ALL cells by performing reciprocal immunoprecipitation experiments (Fig. 2K). To further test specificity of SRSF6 in T-ALL compared to potential roles of other SRSF family members might play, we assayed for protein levels of SRSF3, another member of the SRSF family that also interacts with USP7 (Supplementary Fig. 8E). In contrast to SRSF6, we identified no difference in the SRSF3 levels between HR and NHR cases (Supplementary Fig. 8F). Additionally, our studies did not yield detectable interactions of SRSF6 with other USP proteins such as UPS11 or USP47, which have been shown to interact and/or act together with USP7<sup>74–77</sup> (Supplementary Fig. 8G). SRSF6 consists of one RNA recognition motif (RRM) domain, one RRM homology (RRH) domain and an arginine/serine-rich (RS) domain that mediates protein-protein interaction (Supplementary Fig. 8H). Studies using SRSF6 truncations showed that the RRH domain is required for SRSF6 interaction with USP7 (Supplementary Fig. 8H).

Inhibition of USP7 using the well-studied USP7 inhibitor P5091<sup>78</sup> led to significant reduction of SRSF6 protein levels (Fig. 2L). Silencing of USP7 using short-hairpin RNA in CUTLL1 cells led to a decrease in SRSF6 protein levels similar to P5091 treatment, further underscoring the USP7-mediated regulation of SRSF6 (Fig. 2M, left panel). Treatment of 293T cells with siRNA against USP7 led to a similar reduction in SRSF6 protein levels suggesting a broader biological context for the regulation of SRSF6 by USP7 (Fig. 2M, right panel). Inhibition of global deubiquitinase activity using PR619<sup>79</sup> also led to a significant down-regulation of SRSF6 (Supplementary Fig. 8I), confirming regulation of SRSF6 from the deubiquitinase enzymes. We further show that proteasomal inhibition partially rescues the P5091-mediated reduction in SRSF6 levels (Supplementary Fig. 8J). Additional studies showed that inhibition of NOTCH1 or bromodomain proteins (i.e., MYC) did not affect SRSF6 protein levels (Supplementary Fig. 8K). Gel filtration analysis suggested that SRSF6 might form a complex with USP7 distinct from the USP7 and SF3B1 complex (Supplementary Fig. 8L), suggesting potential participation of USP7 in different splicing complexes.

Gene expression analysis of splicing transcripts in T-ALL cells upon treatment with P5091 showed down-regulation of SRSF transcripts encoding for SRSF proteins and SRSF6 in particular (Supplementary Fig. 8M, N). To differentiate between a potential impact of USP7 in transcriptional versus post-translational regulation of SRSF6, we treated CUTLL1 cells with cycloheximide (CHX) to block translation in the presence or absence of P5091. Analysis of SRSF6 levels showed that the combination of CHX and P5091 treatment leads to a faster decrease in SRSF6 levels compared to CHX alone, suggesting USP7 controls protein level of SRSF6 irrespective of potential effects on *SRSF6* gene transcription (Fig. 2N).

### **SRSF6 levels are critical for leukemia growth**

We then sought out to test the role of SRSF6 as an important USP7 substrate. We ectopically expressed SRSF6 in CUTLL1 cells coupled to treatment with vehicle or P5091 USP7

inhibitor. We show that overexpression of SRSF6 in T-ALL cells leads to a partial rescue of growth inhibition caused by P5091 (Supplementary Fig. 9A). This shows that SRSF6 protein is a biologically relevant substrate of USP7. To confirm this conclusion, we performed genomic silencing of USP7, which led to an inhibition of T-ALL growth. Ectopic expression of SRSF6, rescued USP7 silencing-mediated inhibition of cell growth, confirming data from the P5091 study (Supplementary Fig. 9B, C).

We then silenced *SRSF6* (using the short-hairpin RNA *shSRSF6.0*) in the human T-ALL cell line CUTLL1 to show a significantly diminished growth of T-ALL cells (Fig. 3A). We further showed that even mild reduction of *SRSF6* levels (25–40% silencing) using *shSRSF6.1* and *shSRSF6.2* significantly impairs T-ALL growth *in vitro* (Supplementary Fig. 9D, E), via an increase in apoptosis, accumulation of cells in the G0/G1 phase and reduction of the actively proliferating cell population (Supplementary Fig. 10A, B). To assess the effect of SRSF6 silencing *in vivo* in human-to-mouse xenograft models, we transplanted CUTLL1 T-ALL cells expressing luciferase into immunocompromised mice. Assessment of cell growth using luminescence intensity and two different *shRNAs* for *SRSF6* at different time points showed that silencing of *SRSF6* leads to a delay in tumor growth (Fig. 3B, and Supplementary Fig. 10C; left panel represents quantification of *in vivo* tumor growth over a period of 11 days; right panel depicts bioluminescence photos for representative mice per group are shown) and results in prolonged mouse survival (Fig. 3C). Gene expression patterns showed extensive changes upon SRSF6 silencing, presenting with 543 significantly up-regulated genes and 1001 down-regulated genes (Fig. 3D). Of note, oncogenic targets of NOTCH1 (such as *NOTCH1* and *DELTEX1 (DTX1)*) are among the down-regulated transcripts (Fig. 3D and Supplementary Table 14). KEGG analysis of gene expression changes identified that spliceosome, proteasomal, cell cycle, and oncogenic transcripts are enriched in the alternatively spliced transcript population (Fig. 3E). Changes in spliceosome-related transcript levels suggest that SRSF6 might regulate the levels of other splicing factors. This finding is in agreement with previous studies demonstrating that the activity of splicing factors, such as SRSF1, might control unproductive splicing via NMD of their own and other splicing-related transcripts<sup>53</sup>. Similar to the previously documented role for SRSF proteins in regulating exon skipping, our splicing analysis demonstrated a marked reduction of skipped exons upon *SRSF6* silencing (Fig. 3F). We then interrogated the presence of overlapping alternatively spliced transcripts between USP7 inhibition and SRSF6 silencing that are also changed in T-ALL compared to T cells. We show that there was a significant overlap between transcripts alternatively spliced upon P5091 treatment as well as with transcripts alternatively spliced during the transition from CD3<sup>+</sup> T cells to T-ALL with 342 transcripts commonly affected (Fig. 3G and Supplementary Fig. 10D). This analysis shows that SRSF6 mainly controls exon skipping in transcripts that are alternatively spliced in T-ALL compared to physiological T cells.

### Therapeutic inhibition of splicing in T-ALL

The aforementioned data also suggest that the splicing machinery is aberrantly regulated in T-ALL and inhibition of splicing activity could be a therapeutic avenue in T-ALL. Compounds that inhibit splicing in general and exon skipping in particular, such as the SRSF kinase protein inhibitors, have been studied extensively in blood cancers<sup>2,3,80</sup>. Among them,

the small molecule inhibitor H3B-8800 is the most advanced in terms of translation to bedside, and has been used in clinical trials for acute myeloid leukemia, chronic myelomonocytic leukemia, and myelodysplastic syndrome (NCT02841540)<sup>81</sup>. H3B-8800 and its precursor drug E7107 both inhibit the U2 component SF3B1, and E7107 has been shown to be active against tumors with SRSF2 or SF3B1 mutations<sup>3,81</sup>. We hypothesize that T-ALL cells presenting abnormal splicing landscape might also be sensitive to H3B-8800 and that silencing of SRSF6 might further sensitize them to the drug.

To target the efficacy of splicing inhibition in our model, we treated T-ALL cell lines, including those with wild-type (CUTLL1) and mutant (JURKAT) SF3B1, with H3B-8800<sup>81,82</sup> for 72 h. We included a second cell line with wild-type *SF3B1* (cancer cell line encyclopedia data, DND41 cells). T-ALL cell lines were sensitive to the inhibitor at concentrations similar to other cancer types with splicing mutations<sup>81</sup>, with an IC<sub>50</sub> value of about 30 nM (Fig. 4A). This agrees with previous studies showing that the drug can block the activity of both wild-type and mutant SF3B1-containing spliceosomes<sup>81</sup>. To further validate the effect of H3B-8800 in human T-ALL samples, we analyzed the growth of three diagnostic patient samples treated with H3B-8800 over a 3-day period, via counting live cells in the population. Similar to T-ALL cell lines, the three patient samples were sensitive to H3B-8800 and drug concentrations around 30nM result in significant (>50%) inhibition of cell growth in 3 days (Fig. 4B). We further confirmed these findings in a second group of three diagnostic samples expressing high levels of SRSF6 using the NADPH-based MTT assay upon treatment with vehicle or increasing concentrations of H3B-8800 over a period of 2 days (Supplementary Fig. 11A). Additionally, treatment of mouse lineage-negative Sca/c-kit-positive (LSK) progenitor cells presented with lower lethality upon treatment with H3B-8800 in comparison with mouse T-ALL cells<sup>42</sup> (Supplementary Fig. 11B, C), suggesting a significant therapeutic window. Analysis of the cell cycle and apoptosis changes in both cell lines and patient samples showed a significant dose-dependent increase in apoptosis on day 2 of treatment (Fig. 4C and Supplementary Fig. 11D), and a reduction in the number of dividing cells (Supplementary Fig. 11E–G). Past studies have shown that cancers with splicing mutations exhibit increased sensitivity to splicing inhibitors, potentially due to the essentiality of splicing factors for survival<sup>2,3,15</sup>. To test whether SRSF6 levels affect response to splicing inhibition, we treated control, *shSRSF6.1* and *shSRSF6.2* cells with 30nM H3B-8800 over a period of 72 h. We noticed that cells with lower levels of SRSF6 exhibit increased sensitivity to H3B-8800 treatment compared to control cells (Fig. 4D), in agreement with the effect of inhibitors in splicing factor-mutant cases. These findings suggest aberrant splicing can be a therapeutic vulnerability in T-ALL and a therapeutic implication of SRSF6 functionality in T-ALL.

Analysis of the splicing changes upon treatment of CUTLL1 and JURKAT cells with H3B-8800 over a period of 6 h showed a significant enrichment in exon skipping and intron retention changes, similar to previous reports using H3B-8800 in solid tumors<sup>81</sup> (Fig. 4E and Supplementary Fig. 12A). Splicing analysis upon a longer 24 h treatment of JURKAT cells with H3B-8800 led to conclusions similar to the 6 h treatment (Supplementary Fig. 12B, C). More specifically, proteasomal subunits, such as *PSMB9* and *PSMD4*, are altered whereas the transcript of the proteasome chaperone *PSMG1*<sup>83–85</sup> is the proteasome-related transcript whose splicing is the most significantly altered in H3B-8800-treated cells (Fig. 4F and

Supplementary Fig. 12D). We also sequenced the same libraries for JURKAT cells treated with control (DMSO) or H3B-8800, at 300PE (150/150) using Illumina technology. This showed there are no differences in the splicing changes identified upon use of longer sequencing reads (Supplementary Fig. 12E–G). As the rMATS algorithm we use in our analyses performs better with longer reads, we also employed two additional methods to confirm splicing changes: we used Cufflinks and Cuffdiff for isoform prediction and differential expression analysis of those isoform<sup>86</sup>, a read length-dependent method, as well as the exon usage method DEXSeq that predicts differential exon usage and is read length-independent<sup>87</sup>. In DEXSeq, only the exon coverages are compared regardless of which isoform they belong to. Data analysis showed a significant overlap between transcripts with differentially spliced events from the rMATS analysis, differential isoform expression from the Cuffdiff analysis, and transcripts with differentially used exons from the DEXSeq analysis further underlining the validity of our conclusions drawn from the use of rMATS analysis and suggesting that the most prevalent splicing change between the control (DMSO) and H3B-8800-treated JURKAT cells was exon-related (Supplementary Fig. 12H). The overlapping transcript group is enriched in cell cycle and proteasomal transcripts (Supplementary Fig. 12I). Additionally, we noticed that splicing inhibition affects SRSF6 splicing, leading to a reduced SRSF6 transcript and protein expression (Fig. 4F and Supplementary Fig. 12J, K), further underscoring the interdependency amongst splicing factors. As USP7 controls the stability of SRSF proteins, we sought to study the effect of USP7 inhibition on the splicing landscape in T-ALL cells. In agreement with our previous findings on the impact of USP7 on SRSF biology, we identified a significant change in exon skipping phenomena upon treatment with P5091 USP7 inhibitor (Supplementary Fig. 13A, B). Our studies also show a significant overlap in transcripts affected by splicing in the transition from CD3<sup>+</sup> T cells to T-ALL as well as between H3B-8800- or P5091-treated T-ALL cells and vehicle-treated cells (Fig. 4G and Supplementary Fig. 13C–E). These findings suggest that splicing or USP7 inhibition affect the splicing of critical transcripts that are aberrantly spliced in T-ALL compared to T cells. Gene ontology analysis for the H3B-8800-related splicing alterations in CUTLL1 and JURKAT cells showed an enrichment for spliceosome, DNA damage response and proteasomal transcripts (Fig. 4H).

### **Aberrant splicing of proteasomal subunits can be exploited for therapeutic purposes in T-ALL**

As mentioned above, *PSMG1* is the top alternatively spliced proteasome-related transcript upon H3B-8800 treatment. Further analysis showed that there is an exon 4 skipping event in about 50% (or  $PSI=0.5$ ) of the *PSMG1* transcripts, leading to a switch between two *PSMG1* transcripts in both CUTLL1 and JURKAT cells upon treatment with H3B-8800 (CCDS13660 and CCDS13661, Fig. 5A and Supplementary Fig. 13F). Our gene expression analysis showed a significant decrease in *PSMG1* transcript levels upon treatment with H3B-8800 (see values in y axis representing exon expression levels, Fig. 5A). Targeted PCR analysis using primers flanking *PSMG1* exon 4, confirmed exon 4 skipping upon splicing inhibition via H3B-8800 treatment (Fig. 5B, C). As USP7 controls exon skipping in T-ALL (Supplementary Fig. 13A, B), we studied alterations in *PSMG1* splicing in our data from USP7 inhibition on the splicing landscape in T-ALL cells. In agreement with our previous findings using H3B-8800, P5091 treatment lead to a similar, albeit significantly weaker

compared to H3B-8800 treatment, exon 4 skipping phenotype in *PSMG1* affecting 11% of the transcripts ( $PSI=0.11$ , Fig. 5D and Supplementary Fig. 13G).

Skipping of exon 4 leads to a 21 amino acid deletion (131–152, Supplementary Fig. 14A) yielding the shorter PSMG1–202 isoform. Structure modeling showed that 202 presents with a significant protein structure alteration (Fig. 5E and Supplementary Fig. 14B). As PSMG1 forms a heterodimer with PSMG2 to serve as a chaperone for the core proteasome alpha ring subunits 5 and 7 (PSMA5 and PSMA7)<sup>83,85</sup> critical for proteasome formation, disruption of PSMG1 levels might alter proteasomal function. PSMG1 depleted cells present with incomplete proteasomes and presumably reduced proteasome activities<sup>83,85</sup>. Indeed, our assay for proteasomal activity shows that splicing inhibition significantly impairs proteasomal activity in a drug dose dependent manner (Fig. 5F). Aberrant proteasomal regulation has been implicated in cancer and hematological malignancies in particular, such as in leukemia as well as multiple myeloma<sup>78,88,89</sup>. Higher levels of PSMG1 in T-ALL compared to T cells also suggest a higher proteasomal activity in this disease (Supplementary Fig. 14C). Inhibition of proteasomal function is the frontline therapy in multiple myeloma and it has also been suggested as a therapeutic strategy in preclinical testing in T-ALL and B-cell ALL, mainly via its implications for the regulation of NOTCH1 targets as well as the NF $\kappa$ B pathway<sup>88</sup>. Moreover, USP7 inhibition has been proposed to lead to sensitivity against proteasomal inhibitors in multiple myeloma<sup>78</sup>.

Based on the aforementioned findings, we hypothesized that splicing inhibition can perturb aberrant proteasome function in T-ALL and could act synergistically to proteasome inhibition. To test this hypothesis, we initially showed that T-ALL lines CUTLL1 and JURKAT are sensitive at the nanomolar range of concentrations to the clinically used proteasomal inhibitors bortezomib (Supplementary Fig. 14D). We then asked whether the combination of splicing (H3B-8800) and proteasome (bortezomib or calfrizomib) inhibition could act synergistically in blocking disease growth. We used a range of concentrations for H3B-8800 and calfrizomib or bortezomib in the range of previously used doses in blood and solid tumors<sup>88,90,91</sup>. We noticed an enhanced activity of combinations of H3B-8800 and bortezomib as well as P5091 and bortezomib in suppressing proteasome activity (Fig. 5G and Supplementary Fig. 14E) and a strong synergistic effect against T-ALL cell growth *in vitro* (Bliss analysis<sup>92</sup>, Fig. 5H and Supplementary Fig. 14F). Use of a calfrizomib and H3B-8800 combination led to similar conclusions (Supplementary Fig. 14G).

To test the therapeutic window of the combinatorial treatment, we treated human CD34<sup>+</sup> hematopoietic progenitor cells from the cord blood with H3B-8000, bortezomib and their combination. Initially, we noticed that CD34<sup>+</sup> are less sensitive than T-ALL patient samples and cell lines at the 30nM H3B-8800 concentration (Supplementary Fig. 15A and comparison to Fig. 4A, B). Although CD34<sup>+</sup> cells are sensitive to bortezomib treatment at concentrations similar to T-ALL samples (Supplementary Fig. 15B), treatment of CD34<sup>+</sup> with doses of bortezomib and H3B-8800 that synergistically lead to a significant inhibition of T-ALL growth (see heatmap in Fig. 5H) led to a very mild effect on CD34<sup>+</sup> growth (Supplementary Figs. 15C, D).

To assess a potential role for the PSMG1 exon 4 skipping in therapy resistance, we designed antisense oligos (ASO) with the aim to block exon skipping and thus block an increase of the 202 isoform of *PSMG1* upon application of H3B-8800 onto T-ALL cells. By using different combinations of two different ASOs, we managed to partially block exon 4 skipping of *PSMG1* (~25% reduction in 202 allele, Supplementary Fig. 15E–G). Treatment with bortezomib as well as the splicing inhibitor H3B-8800 both presented with a decreased sensitivity of the ASO-expressing cells towards therapy suggesting that further modulation of *PSMG1* splicing might pave the way for therapeutic intervention in acute leukemia (Supplementary Fig. 15H and I).

## DISCUSSION

In this study, we characterized splicing changes and associated molecular underpinnings in T-ALL. Our findings suggest that USP7 controls the post-translational levels of SRSF6 factors in T-ALL leading to aberrant splicing regulation (Fig. 6). Our study reinforces findings in recent studies in blood and other malignancies that there is extensive aberrant splicing in cancer in the absence or presence of mutations affecting the splicing machinery<sup>5,13,93,94</sup>. We show that the transcripts affected by abnormal splicing include cell cycle-related proteins, epigenetic modifiers, and proteasomal subunits, all of which represent therapeutic vulnerabilities in this disease.

Our study compares a differentiated total T cell population (CD3<sup>+</sup>) or the CD4<sup>+</sup> T cell subset from the peripheral blood to undifferentiated thymocytes. We show that CD3<sup>+</sup> and CD4<sup>+</sup> T cells present with similarities in the splicing landscape and splicing phenomena distinct from thymocytes, with an extensive number of cell cycle-related transcript differentials between thymocytes and differentiated CD3<sup>+</sup>/CD4<sup>+</sup> T cells. Thus, splicing might reflect the developmental stage of T cells. In addition, T cells were significantly different from T-ALL patient cells with regards to the splicing landscape, and disease cases with high risk for relapse (“high-risk”) exhibited a significant number of mutually exclusive exons and skipped exon phenomena different from the non-high risk cases suggesting that splicing might be a good indicator of disease status.

Proteasome, cell cycle and epigenetic enzymes are critical gene ontology terms significantly altered between T cells and the different disease subtypes. In the current study, we identified components of the 20S and 19S proteasome as well as the proteasome chaperone PSMG1 that are differentially spliced in T-ALL compared to T cells. In silico modeling of PSMG1 structure showed extensive changes in protein structure in T-ALL and our experiments demonstrate that inhibition of the splicing machinery affects proteasomal function. We further show that the components of the splicing machinery might be regulated at the post-translational level via the activity of deubiquitinases and we present regulation of SRSF6 by USP7 as a proof of principle. Hitherto, efforts towards understanding splicing factor regulation in cancer at the non-genetic level have mainly focused on transcriptional control via oncogenic factors such as MYC<sup>19,68</sup>. Additionally, our findings suggest that SRSF6 might be regulated via NMD T cells but not in T-ALL, as we noticed a significant reduction of the NMD-related allele in T-ALL and its re-appearance upon silencing of the UPF1 component of the NMD machinery<sup>52,53</sup> (Supplementary Fig. 3c–g). Further investigation is

required to properly address the role of the NMD process upon SRSF levels in T-ALL as well as potential feed forward loops between transcriptional regulation, NMD, and post-translational regulation.

Although post-translational modifications, such as methylation via arginine methyltransferases and phosphorylation via SRSF protein kinases in particular, have been previously suggested as a means of regulating splicing factor activity<sup>67,80,95–99</sup>, there is very little information on how ubiquitination or similar modifications controls splicing factor levels or activity<sup>72,73,100–104</sup>, especially in cancer systems. Further investigation is warranted to identify and characterize different types of splicing factor ubiquitination and whether it mediates effects other than regulation of the protein levels. We further show that modulation of USP7 activity or SRSF6 levels leads to changes in the expression or/and splicing pattern of the transcripts of other splicing factors. This suggests that SRSF6 regulates the levels of other splicing transcripts. Indeed, it has been reported in the past that a few initial changes in the activity or levels of splicing factors can subsequently lead to extensive changes to the splicing landscape of spliceosome transcripts via controlling unproductive splicing leading to non-sense-mediated decay<sup>53</sup>. Spliceosome-related transcript changes with regards to splicing and expression between cancer and physiology as well as upon splicing inhibition might be similarly explained via alterations in the levels of SRSF6 or SF3B1 (in the case of H3B-8800). These findings warrant further investigation in cancer.

In the realm of blood cancers, clinical trials have been evaluating the potential of splicing-targeted compounds in myeloid malignancies and pre-malignant lesions. Similar therapeutic approaches might be employed in T-ALL, a disease without splicing factor mutations. We show that treatment with splicing or deubiquitinase inhibitors affect splicing in disease-related transcripts and blocks T-ALL growth. Our study extends the findings of previous studies suggesting that targeting protein levels of SF3B1 via blocking deubiquitination could be exploited in cancers with SF3B1 mutations<sup>105</sup>. We demonstrate that deubiquitination actively controls splicing factor stability and inhibition of deubiquitination can be a valid therapeutic strategy in cancer in the presence or absence of splicing mutations. To assess whether splicing inhibition could act in a combinatorial fashion with other drugs currently in use in preclinical or clinical practice, we used combinations of proteasomal and splicing inhibitors as well as deubiquitinase and splicing inhibitors to demonstrate a synergistic effect in inhibiting leukemia growth. Similar to previously suggested alternative methods of targeting the splicing machinery, including arginine methyltransferase inhibitors<sup>97,98</sup>, our study elucidated a method of targeting splicing via inhibition of deubiquitination and paves the way for further testing this therapeutic modality in additional cancer types with or without splicing factor mutations. Our studies also suggest a potential therapeutic window upon combinatorial drug treatment as H3B-8800 and combination with proteasome inhibition are not similarly efficient in inhibiting normal mouse and human hematopoietic progenitors growth *in vitro*. This conclusion is in agreement with recent clinical data using H3B-8800, that suggest that the drug might be safe even after prolonged dosing<sup>106</sup>. Additional preclinical studies are warranted to evaluate the toxicity and efficacy for the use of combinations of splicing and proteasomal inhibitors.

Whether SRSF proteins functionally and physically interact with oncogenes or pro-oncogenic co-factors to regulate splicing or other RNA-related processes, including transcriptional elongation, is hitherto relatively undercharacterized. A recent study showed that BRD4 might coordinate splicing and transcriptional elongation via interaction with the splicing machinery<sup>51</sup>. SRSF proteins, including SRSF6, have not been identified as NOTCH1 interactants in published NOTCH1 mass spectrometry studies<sup>107,108</sup> and our studies show that NOTCH1 inhibition does not affect SRSF6 levels. Nevertheless, the role of NOTCH1, and potentially other oncogenes, in the transcriptional and post-translational regulation of SRSF proteins nonetheless warrants further investigation.

In conclusion, our study provides new proof-of-principle for post-translational regulation of SRSF, independently of splicing factor mutations, and suggests new combinatorial treatment in leukemia - a concept that might apply to additional tumors in the presence or absence of splicing mutations.

## METHODS

### Cell lines and primary cells

The human T-ALL cell lines CUTLL1 (gift from Adolfo Ferrando, Columbia University), JURKAT (American Type Culture Collection (ATCC), Manassas, VA, #CCL-119), and DND41 (ATCC) were cultured in RPMI 1640 medium supplemented with 10% heat-inactivated FBS (Sigma-Aldrich, St. Louis, MO), 2% penicillin/streptomycin (Gibco, Fisher Scientific, Hampton, NH), 1% GlutaMAX (Gibco, Fisher Scientific). 293T cells (ATCC, #CRL-11268) were maintained in DMEM medium supplemented with 10% heat-inactivated FBS, 2% penicillin/streptomycin, and 1% GlutaMAX. The cells are periodically tested for the presence of mycoplasma using the Lonza Walkersville MycoAlert Mycoplasma Detection Kit (last test on 01.2020). The cell lines are kept in culture for a maximum of 20 passages and are authenticated using short-tandem repeats profiling (JURKAT and DND41) or using PCR to detect the TCRb-NOTCH1 translocation (*TCRBJ2S4CUTLL1F:5'*-GGACCCGGCTCTCAGTGCT-3', *NOTCH1CUTLL1R:5'*-TCCCGCCCTCCAAAATAAGG-3'). Last cell authentication was performed in February of 2020. Human CD3<sup>+</sup>, CD8<sup>+</sup> and CD4<sup>+</sup> T cells were purchased from [AllCells.com](https://www.allcells.com) (Alameda, CA) or from Astarte Biologics (Bothell, WA). Primary human samples were collected by collaborating institutions with written informed consent and analyzed under the supervision of the Institutional Review Board of Padova University, the Associazione Italiana Ematologia Oncologia Pediatrica, and the Berlin-Frankfurt-Münster (AIEOP-BFM) ALL 2000/2006 pediatric clinical trials. Written informed consent for the use of leftover material for research purposes was obtained from all of the patients at trial entry in accordance with the Declaration of Helsinki.

### Antibodies and reagents

The following antibodies were used for western blotting or immunoprecipitation: mouse anti-actin (Millipore, Billerica, MA, clone C4), rabbit anti-SRSF6 (Bethyl Laboratories, Montgomery, TX, A303-669A, and Abcam, Cambridge, UK (ab140602)), rabbit anti-SRSF3 (Abcam, ab73891), rabbit anti-SF3B1 (MLB, Woburn, MA (D221-3)), rabbit anti-



USP7 (Bethyl Laboratories, Montgomery, TX (A300–033A-7)), rabbit anti-cleaved NOTCH1 (Val1744) (Cell Signaling Technology, Danvers, MA (4147)), and rabbit anti-Lamin B1 (Proteintech Group, Rosemont, IL (12987–1-AP)). HA antibody (C29F4, Cat. No. 3724) was purchased from Cell Signaling Technologies. Secondary antibodies for western blots were HRP-conjugated anti-rabbit and anti-mouse IgG (GE Healthcare, Chicago, IL). Quick Start Bovine Gamma Globulin (BGG) Standard Set protein standards were purchased from Bio-Rad (Hercules, CA). Benzonase nuclease, RNase A, and dithiothreitol (DTT) were purchased from Sigma-Aldrich. NaV and NaF were purchased from New England BioLabs (Ipswich, MA). Protein G Dynabeads were purchased from Life Technologies (Carlsbad, CA). IgG-free BSA was purchased from Jackson ImmunoResearch Laboratories (West Grove, PA). Phenol chloroform was purchased from ThermoScientific (Waltham, MA). Proteinase K, Tousimis formaldehyde, and MG132 reagent were purchased from Fisher Scientific. USP7 inhibitor P5091 was purchased from Selleckchem (Houston, TX). H3B-8800 was obtained through collaboration with H3 Biomedicine (Cambridge, MA).

### Gel filtration and immunoprecipitation

Gel filtration was performed using whole cell extracts and a Superose 6 column to separate complexes from 5MDa to 5KDa. Immunoprecipitation and mass spectrometry studies were performed as described previously<sup>70</sup>: 200 million cells were incubated in TENT buffer (50 mM Tris pH 7.5, 5 mM EDTA, 150 mM NaCl, 0.05% v/v Tween 20, 1:100 protease inhibitor (Sigma-Aldrich, P8340), 1 mM NaV, 1 mM NaF, and 0.5 mM DTT in H<sub>2</sub>O) supplemented with 5 mM MgCl<sub>2</sub> and 100 units benzonase, and incubated at 4°C for 30 min, with rotation. Lysates were passed through a 25<sup>1/2</sup>G needle/syringe 3 times, and spun down at 4°C, 2,000 RPM, for 7 min to remove debris. Lysates were then incubated with the appropriate antibody-conjugated beads (15 µg antibody) at 4°C overnight, with rotation. Beads were washed 4 times in TENT buffer at 4°C for 3 min, and protein complexes were eluted in 50 µL 0.1 M glycine, pH 2.5, for 10 min at 25°C, with shaking, followed by addition of 5 µL of 1 M Tris pH 8.0 to the supernatants.

### Sample Preparation for Mass Spectrometry

Immuno-precipitated proteins were processed for acetone precipitation and the purified protein pellet was denatured in 50µL of 8M Urea/0.4M Ammonium Bicarbonate followed by reduction in 2µL of 100mM DTT. Protein was alkylated with 18mM iodoacetamide for 30 min at room temperature in the dark. Samples were diluted with four volumes of water to bring urea concentration to 1.8 M. Sequencing-grade trypsin (Promega) was added at 1:50 (enzyme: substrate) and incubated at 37°C overnight. The digests were acidified to 0.5% trifluoroacetic acid (TFA) and the peptides were desalted on C18 Sep-Paks (Waters). Peptides were eluted with 2X 50uL of 80% ACN/0.1% TFA to ensure complete recovery. The pooled extracts were dried in a vacuum concentrator and resuspended in 30 uL of 5% ACN/0.1% FA for LC-MS analysis.

For the ubiquitin analysis, PTMScan® Ubiquitin Remnant Motif (K--GG) Kit was used following manufacturer's instruction (Cell Signaling Technology, Inc, Danvers, MA).

## LC-MS/MS Analysis

Peptides were analyzed by LC-MS/MS using a Dionex UltiMate 3000 Rapid Separation nanoLC and either an Orbitrap Velos Mass Spectrometer or QEHF (Thermo Fisher Scientific Inc, San Jose, CA). Samples were loaded onto the trap column, which was 150  $\mu\text{m}$  x 3 cm in-house packed with 3  $\mu\text{m}$  ReproSil-Pur® beads. The analytical column was a 75  $\mu\text{m}$  x 10.5 cm PicoChip column packed with 3  $\mu\text{m}$  ReproSil-Pur® beads (New Objective, Inc. Woburn, MA). The flow rate was kept at 300nL/min. Solvent A was 0.1% FA in water and Solvent B was 0.1% FA in ACN. The peptide was separated on a 120-min analytical gradient from 5% ACN/0.1% FA to 40% ACN/0.1% FA. Previously selected ions were dynamically excluded from re-selection for 60 seconds. Proteins were identified from the MS raw files using the Mascot search engine (Matrix Science, London, UK. version 2.5.1). MS/MS spectra were searched against the SwissProt human database. All searches included carbamidomethyl cysteine as a fixed modification and oxidized Met, deamidated Asn and Gln, and acetylated N-term as variable modifications. Di-glycine on Lys was set as a variable modification for ubiquitin detection. Three missed tryptic cleavages were allowed. A 1% false discovery rate cutoff was applied at the peptide level. Only proteins with a minimum of two peptides above the cutoff were considered for further study. Identified peptides/protein were visualized by Scaffold software (version 4.9.0, Proteome Software Inc., Portland, OR).

## Immunoblots and reverse phase protein array (RPPA)

Up to 10 million cells were collected to prepare whole-cell extracts, as described previously<sup>70</sup>, and resuspended in 40  $\mu\text{L}$  RIPA buffer (50 mM Tris HCl pH 8.0, 150 mM NaCl, 1% NP-40/IGEPAL, 0.5% sodium deoxycholate, 0.1% SDS, 1:100 protease inhibitor (Sigma-Aldrich, P8340), 1 mM NaV, and 1 mM NaF in H<sub>2</sub>O) per 2 million cells. RPPA was performed as described previously<sup>70,109,110</sup>. Briefly, cells were lysed in an appropriate lysis buffer with protease and phosphatase inhibitors, serially diluted into four-points dilution curves, and printed on nitrocellulose-coated glass slides using the Aushon 2470 Arrayer (Aushon Biosystems).

## CRISPR/Cas9 screen

A previously described single-guide RNA (sgRNA) domain-focused approach was used in the screen, which enhances CRISPR/Cas9-negative selection by targeting a functional protein domain. Individual sgRNAs were subcloned into a lentivirus-based GFP-tagged sgRNA vector and transfected into different types of tumor cell lines for a loss-of-function pooled screen. Genomic DNA was harvested from cells on day 4 and day 20 post transduction of sgRNA library, and individual sgRNA read counts were evaluated by next-generation sequencing. Changes in sgRNA abundance were assessed by measuring the average fold change (day4/day20) of all sgRNAs targeting a given gene.

## Targeted sequencing

The library was captured with Nimblegen SeqCap (Madison, WI) and sequenced using Illumina technology. The alignment was done by Burrows-Wheeler Aligner (BWA) and the variants called by genome analysis toolkit (GATK) and annotated using the single nucleotide polymorphism database (dbSNP) and SnpEff. The variant filtered for impact (high or

moderate) and checked for missense mutations in the coding sequence of our genes using Integrative Genomics Viewer (IGV).

### RNA isolation, sequencing and PCR

RNA was extracted from cell lines and patient samples using Bio-Rad total RNA isolation kit. Poly(A)-selected, unstranded Illumina libraries were generated using the TruSeq RNA kit from Illumina. Library fragments were amplified with PCR (15 cycles), size selected using AMPure XP beads to select for fragments between 200 and 500 bp, and sequenced on the Illumina NextSeq 500 in a paired-end run ( $2 \times 76$ -bp) for a sequencing depth of about 80 million reads per sample.

Primers:

PSMG1-F: TGGGAGGAAGTTGGTTGTGC

PSMG1-R: GGACAACACGCCGAGTCTTT

SRSF2-exon2-F: CTATGGATGCCATGGACGGG

SRSF2-exon2-R: CTCCGTTTACTGCTTGCC

SRSF6-exon3-F: GACGGCTACAGCTACGGAAG

SRSF6-exon3-R: GCCAACTGCACCGACTAGAA

SRSF7-cryptic-F: TGCAGAAGATGCAGTACGAGG

SRSF7-cryptic-R: AGCGAGAGTATCGCCTTCCT

Real time primers:

SRSF6-NMD-F CTTTGGCTGACCTTACCGGA

SRSF6-NMD-R TCCGACTGCTGTATCCACCT

Antisense oligos (ASO) designed to block exon skipping in PSMG1:

ASO1: 0120\_1739\_2OM\_E4 5' -

mC\*mC\*mU\*mG\*mG\*mC\*mU\*mC\*mC\*mA\*mC\*mU\*mA\*mU\*mU\*mG\*mA\*mC\*mC  
\*mU\*mA\*mC - 3'

ASO2: 0120\_1740\_2OM\_E4 5' -

mA\*mA\*mG\*mU\*mU\*mC\*mC\*mA\*mC\*mG\*mC\*mU\*mU\*mU\*mU\*mU\*mG\*mU\*m  
C\*mA\*mA\*mG\*mU\*mA\*mA\*mG\*mU\*mU\*mU\*mU\*mA\*mU\*mA\*mC\*mA\*mC\*mA -  
3'

The positive control ASO is designed to promote exon skipping of C1orf43 gene:

CAU CCA GAG CUU UCA UCC UAU ACA GAU AGU UG.

The following information was taken into considerations upon designing the ASO: a) Every base is 2' O-Methyl RNA, b) Every base is linked by phosphorothioate bond, c) we performed a 100nM synthesis scale coupled to HPLC purification. ASO transfection was performed using 100nM or 200nM final concentration of each ASO based on the Lipofectamine 3000 Transfection reagent from Thermo Scientific (Waltham, MA) following manufacturer's guidelines. In brief, 6 microliters of P3000 and 6 microliters of lipofectamine for each condition to transfect 800,000 T-ALL cells per well of a 6-well plate.

### Bioinformatics analysis

RNA sequencing reads were mapped to human genome hg19 using TopHat. Differential gene expression analysis was performed using the EdgeR package in R. Gene expression changes were visualized in heatmaps using the ggplot2 package in R. rMATS version 4.0.2 was used to perform alternative splicing analysis with human Ensembl.GRCh37v75 as the annotation. The exon count tables and differential exon usage was calculated using DEXSeq (v3.10)<sup>87</sup>. Isoform predictions and isoform differential expression analysis were analyzed using Cufflinks and Cuffdiff (v 2.2.1) (PMID: 20436464)<sup>86</sup>. In all related figures, rMATS bargraphs present events that passed the statistical threshold (FDR controlled P value < 0.05) and percent spliced in (PSI) > 0.1). To compare the level of similarity among the samples and their replicates, we used two methods: principal-component analysis and Euclidean distance-based sample clustering. Enriched Kyoto Encyclopedia of Genes and Genomes (KEGG) pathways and gene ontology terms were identified using gene set enrichment analysis (GSEA)<sup>111</sup> or EnrichR<sup>112</sup>. Bubble charts representing enrichment analysis were generated using the pathfindR package in R. Venn diagrams of overlaps were generated using an online Venn diagram generator (<https://www.meta-chart.com/venn>).

### Analysis of data from publicly available databases

Analysis of microarray data from Gene Expression Omnibus (GEO) was done using the NCBI GEO2R online tool for microarray analysis. Quantile normalization was used to process microarray data. Adjusted p-value calculations were done using the Benjamini & Hochberg option. A P value of <0.05 was considered to be statistically significant. Gene essentiality data for cancer cell lines was obtained from the Project Achilles CRISPR-Cas9 screening dataset (<https://depmap.org/portal/download/>; 2019 Quarter 2 release). Essentiality of individual genes is represented as the inverse of the CERES score for that gene<sup>113</sup>. Visualization of gene essentiality data was achieved in Python (version 3.6.4, Anaconda Inc.) using the modules Pandas (v0.23.4) and Seaborn (v0.9.0).

### Cell transfection and virus production

293T cells that reach up to 70% confluency were used for transfection using jetPrime reagent followed the recommended protocol (Polyplus, France). After 48 h, 293T cells were collected for the subsequent experiment as required. The following short-hairpin RNAs (Sigma-Aldrich, MISSION system) were used:

*shUSP7.1:5'*-CCGGCCTGGATTTGTGGTTACGTTACTCGAGTAAC  
GTAACCACAAATCCAGGTTTTT-3',

*shUSP7.2*: 5'-  
CCGGCCAGCTAAGTATCAAAGGAACTCGAGTTTCCTTTGATACTTAGCTGGTTTT  
T-3',

*shSRSF6.0*: 5'-  
CCGGCGAACAAATGAGGGTGTAATTCTCGAGAATTACACCCTCATTTGTTTCGTTTT  
TG-3' (TRCN0000231443, NM\_006275.4-589s21c1),

*shSRSF6.1*: 5'-  
CCGGGCTCCCATTACATTCTCGAACTCGAGTTCGAGAATGTGAATGGGAGCTTT  
TT-3' (TRCN0000006624, NM\_006275.4-923s1c1)

and *shSRSF6.2*: 5'-  
CCGGGGCAGAAATATTAGGCTTATTCTCGAGAATAAGCCTAATATTTCTGCCTTTTT  
G-3' (TRCN0000231444, NM\_006275.4-673s21c1).

Non-mammalian *shRNA control* hairpin SHC002 5'-  
CCGGCAACAAGATGAAGAGCACCAACTCGAGTTGGTGCTCTTCATCTTGT  
TGTTTTT-3' was used.

*siRNA* against USP7 was a SMARTpool of the following ON-TARGETplus siRNAs: siRNA J-006097-05 (Target Sequence: AAGCGUCCCUUAGCAUUA), J-006097-06 (GCAUAGUGAUAAACCUGUA), J-006097-07 (UAAGGACCCUGCAAUUAU), J-006097-08 (GUAAAGAAGUAGACUAUCG). The siRNA control (Silencer negative control #1, 4390843) was purchased from ThermoFisher Scientific.

For SRSF6 overexpression, the SRSF6 ORF was cloned (using BamHI/XhoI) into the Phage vector backbone and the gene is expressed under the CMV promoter. Additionally, SRSF6 overexpression vector used in the study was also purchased from Horizon Discovery (Cambridge, UK): *SRSF6*: Precision LentiORF SRSF6, PLOHS\_ccbBEn\_069 BC006832 BC006832.2 37

The Precision LentiORF USP7 (PLOHS\_100066416 BC166690, Horizon Discovery (Cambridge, UK)) was used for *USP7* expression in leukemia cells.

Control expression vector: Precision LentiORF RFP Positive control E2017121504 (Horizon Discovery (Cambridge, UK))

Inducible short-hairpin RNAs from Horizon Discovery:

*shUPF1* (TRIPZ Inducible Lentiviral shRNA):

*shUPF1.1*: RHS4696-200708840 (pTRIPz, TURBORFP, clone ID, V2THS\_32895)

*shUPF1.2*: RHS4696-200681171 (pTRIPz, TURBORFP, Clone Id: V2THS\_32893)

*shUSP7* (SMARTvector Inducible Lentiviral):

*shUSP7*: V3SH7669–227599723 (Clone Id: V3IHSHER\_7537373)

Control vector for the silencing studies: TRIPZ Inducible Lentiviral Non-silencing shRNA Control (RHS4743). The Dharmacon Trans-Lentiviral ORF Packaging kit with calcium phosphate transfection reagent was used for the transfection of all Dharmacon related constructs following manufacturer's recommendations. Viruses were used to infect T-ALL cells as previously described<sup>70,114</sup>.

### **Assays: Cell growth and viability assays, apoptosis, cell cycle analysis, MTT, and proteasome activity**

To study cell growth, 3,000 cells per well were seeded using a microplate dispenser (MultiFlo™, BioTek, Winooski, VT) in 384-well clear bottom, black wall plates (Corning, Corning, NY), and drugs were added using the Tecan D300e digital dispenser (Tecan, Mannedorf, Switzerland). After 72 h incubation, alamarBlue™ cell viability reagent (ThermoFisher, Waltham, MA) was added and viability was quantified by measuring fluorescence in a plate reader (Tecan Infinite m1000 pro,  $\lambda_{ex}$ : 530 nm;  $\lambda_{em}$ : 590 nm). A total of 500,000 cells were plated in each well of a 24-well plate. For apoptosis analysis, cells were stained with LIVE/DEAD Fixable Near-IR Dead Cell Stain (Life Technologies, Carlsbad, CA) according to the manufacturer's protocol, except that cells were stained for 20 min at 4°C, prior to staining with PE-conjugated annexin V (Life Technologies) in

Annexin V Binding Buffer (BD Biosciences, San Jose, CA) according to the manufacturer's instructions. Fortessa cytometer was used for signal detection. For cell cycle analysis, cells were fixed in 100  $\mu$ L Fix and Perm Medium A (Life Technologies) for 15 min, washed with PBS, and incubated with 0.1% Triton in 1x PBS, supplemented with 1  $\mu$ g/mL DAPI (Invitrogen, Carlsbad, CA) for 6 h at 4°C. Flow cytometry was performed on an LSR II (BD, Franklin Lakes, NJ) and analyses were performed using FlowJo software (Tree Star, Ashland, OR). Statistical analyses were performed using GraphPad Prism software (GraphPad Software, CA) using Student's unpaired, two-sided t-test or Dunn's multiple comparison test.

Cell viability was assessed by MTT ((3-(4,5-dimethylthiazol-2-yl)-2,5-diphenyl tetrazolium bromide) assay. We seeded 100,000 patient cells and 25,000 cells per well in a 96-well plate. At the end of the treatment period, we added 10  $\mu$ l 5mg/ml MTT and the cells were incubated for 4 h followed by the addition of 100  $\mu$ l of isopropanol:HCL=500:3.3 mix per well and the absorbance was measured (560nm). The Growth Inhibition 50 (GI50, compound concentration required to inhibit cell growth by 50%) was calculated by plotting the data as a logarithmic function of when viability was 50%. Control cells viability was set to 100%.

For CD34<sup>+</sup>, M106, M114 and M181 cell growth analysis, we used cytometry and Via Count kit to remove dead cells (<https://www.luminexcorp.com/guava-viacount-reagent-40ml/>) and we then gated on single live cells. Staining with hCD45 and hCD7 antibodies was used for the counting of the patient cells.

The Promega chymotrypsin-like kit (G8660) was used to assay proteasomal activity.

### Ubiquitination assays

293T cells were transfected with HA-Ubiquitin or Flag-SRSF6 and treated with either DMSO or 10  $\mu$ M P5091 USP7 inhibitor for 24 h. Cells were harvested and lysed and SRSF6 was pulldown using Flag antibody. Proteins were eluted prior to western blotting, for detection of ubiquitin levels using HA antibody.

### Drug synergism

A total of 3,000 cells per well were seeded using a microplate dispenser (MultiFlo™, BioTek) in 384-well clear bottom, black wall plates (Corning). Drugs were added using the Tecan D300e digital dispenser (Tecan). After 72 h incubation, alamarBlue™ cell viability reagent (ThermoFisher) was added and viability was quantified by measuring fluorescence in a plate reader (Tecan Infinite m1000 pro,  $\lambda_{\text{ex}}$ : 530 nm;  $\lambda_{\text{em}}$ : 590 nm). Synergy analysis was conducted using SynergyFinder software and the Bliss Independence model<sup>92,115</sup>.

### Homology model building for PSMG1–201 and PSMG2 –202 and their validations

The primary amino acids sequences for PSMG1–201 and PMG2–202 having the accession codes NP\_003711.1 and NP\_982257.1 were obtained from NCBI database. The PSMG1 protein contains 288 amino acids and PSMG2 is a truncated version of PSMG1 missing a loop of 20 amino acids. We subjected the two query sequences to BLAST/PSI-BLAST engines and obtained homologous (template) structures. Analyzing the template structures, we found that none of them have a sequence identity > 40 % to both query sequences, which ruled out the possibility of building a single template-based comparative homology model for PSMG1 and PSMG2. Hence, we utilized a multiple template-based homology building tool to generate the models. The different parts of the query sequences were assigned to different template structures to build the models. The Prime 3.1 module implemented in Schrodinger platform<sup>116</sup> was used to build the models. Prime 3.1 is a well-validated protein structure prediction program that integrates comparative modeling and fold recognition into a single interface. The comparative modeling techniques include template identification, alignment, and final model building. Furthermore, it also allows the refinement of the side chains, loops, and minimizes the free energy. Based on the template structures, two consensus homology models were built for PSMG1 and PSMG2.

After building models using Prime3.1, we carried out further energy minimization steps using the MacroModel tool available in Schrodinger suite<sup>117</sup>. The energy minimized models were then subjected to All-Atoms MolProbity validations<sup>118</sup>. The MolProbity validation reveals that both the model structures have < 3 % clash scores, <5% poor rotamers and > 90% favorable residues in the Ramachandran plot. Finally, no residue was found to have non-favorable dihedral angles or steric collisions. When we superposed both structures, we found structural deviations between the two as the PSMG2 structure is missing a 20 amino acid loop. The calculated root mean square deviation (RMSD) between the two models was found to be ~ 2.5 Å.

## Intravenous and subcutaneous xenograft studies

All mice were housed in a barrier facility, and procedures were performed as approved by the Northwestern University Institutional Animal Care and Use Committee (protocol Ntziachristos #IS00002058 and Mazar #IS00000556).

For CUTLL1 T-ALL intravenous studies, 1 million cells in 100  $\mu$ l PBS were injected into the tail vein of 8-week-old NOD.Cg-Prkdcscid male mice (#005557, Jackson Laboratories, Portage, MI). Body weight and tumor size (via calipers) were measured 3 times per week. Animals were monitored by IVIS every 3 days for luciferase signal detection. IVIS images were taken using the IVIS Spectrum *in vivo* imaging system (PerkinElmer). For statistical analyses, mouse hosts with changes in luciferase values greater or less than the interquartile range of each dataset multiplied by 1.5 were considered outliers and excluded from the study.

## Supplementary Material

Refer to Web version on PubMed Central for supplementary material.

## Acknowledgments

The Ntziachristos laboratory is or has been supported by the National Cancer Institute (R00CA188293 and R01CA248770), the National Science Foundation, the Hartwell Foundation, a Gilead Research Scholarship, the American Society of Hematology, the Leukemia Research Foundation, the St. Baldrick's Foundation, the H Foundation, the Gabrielle's Angel Foundation, the Elsa Pardee Foundation, and the Zell Foundation. B.T.G.D. has been supported by the Fulbright Foundation and The Graduate School of Northwestern University. D.R.A. was supported by 5T32GM008152-33. Proteomics services were performed by the Northwestern Proteomics Core Facility, supported by NCI CCSG P30 CA060553 awarded to the Robert H Lurie Comprehensive Cancer Center, instrumentation award (S10OD025194) from NIH Office of Director, and the National Resource for Translational and Developmental Proteomics supported by P41 GM108569. A.T. is supported by the American Cancer Society (RSG-15-189-01-RMC), St. Baldrick's foundation (581357) and NCI/NIH P01CA229086-01A1. We thank the NYU Langone Genome Technology Center (GTC) for PacBio Sequel sequencing, acquired with the Shared Instrumentation Grant 1S10OD023423-01 from NIH. We also thank the Applied Bioinformatics Laboratories (ABL) for providing bioinformatics support and helping with the analysis and interpretation of the data. GTC and ABL are shared resources partially supported by the NYU Cancer Center Support Grant P30CA016087 at the Laura and Isaac Perlmutter Cancer Center. This work has used computing resources at the NYU School of Medicine High Performance Computing Facility. We want to thank Dr. Issam Ben Sahra and laboratory and the Department of Biochemistry and Molecular Genetics for helping with reagents and equipment used in the study as well as all the members of the Ntziachristos laboratory for their comments and critical review of the manuscript.

## REFERENCES

1. Wang ET et al. Alternative isoform regulation in human tissue transcriptomes. *Nature* 456, 470–476, doi:10.1038/nature07509 (2008). [PubMed: 18978772]
2. Kim E et al. SRSF2 Mutations Contribute to Myelodysplasia by Mutant-Specific Effects on Exon Recognition. *Cancer Cell* 27, 617–630, doi:10.1016/j.ccell.2015.04.006 (2015). [PubMed: 25965569]
3. Lee SC et al. Modulation of splicing catalysis for therapeutic targeting of leukemia with mutations in genes encoding spliceosomal proteins. *Nat Med* 22, 672–678, doi:10.1038/nm.4097 (2016). [PubMed: 27135740]
4. Ntziachristos P, Abdel-Wahab O & Aifantis I Emerging concepts of epigenetic dysregulation in hematological malignancies. *Nat Immunol* 17, 1016–1024, doi:10.1038/ni.3517 (2016). [PubMed: 27478938]



5. Dvinge H, Kim E, Abdel-Wahab O & Bradley RK RNA splicing factors as oncoproteins and tumour suppressors. *Nature reviews. Cancer* 16, 413–430, doi:10.1038/nrc.2016.51 (2016). [PubMed: 27282250]
6. Inoue D & Abdel-Wahab O Modeling SF3B1 Mutations in Cancer: Advances, Challenges, and Opportunities. *Cancer Cell* 30, 371–373, doi:10.1016/j.ccell.2016.08.013 (2016). [PubMed: 27622329]
7. Shirai CL et al. Mutant U2AF1 Expression Alters Hematopoiesis and Pre-mRNA Splicing In Vivo. *Cancer Cell* 27, 631–643, doi:10.1016/j.ccell.2015.04.008 (2015). [PubMed: 25965570]
8. Yoshimi A & Abdel-Wahab O Molecular Pathways: Understanding and Targeting Mutant Spliceosomal Proteins. *Clin Cancer Res* 23, 336–341, doi:10.1158/1078-0432.CCR-16-0131 (2017). [PubMed: 27836865]
9. Yoshimi A et al. Coordinated alterations in RNA splicing and epigenetic regulation drive leukaemogenesis. *Nature* 574, 273–277, doi:10.1038/s41586-019-1618-0 (2019). [PubMed: 31578525]
10. Inoue D et al. Spliceosomal disruption of the non-canonical BAF complex in cancer. *Nature* 574, 432–436, doi:10.1038/s41586-019-1646-9 (2019). [PubMed: 31597964]
11. Papaemmanuil E et al. Somatic SF3B1 mutation in myelodysplasia with ring sideroblasts. *The New England journal of medicine* 365, 1384–1395, doi:10.1056/NEJMoa1103283 (2011). [PubMed: 21995386]
12. Rossi D et al. Mutations of the SF3B1 splicing factor in chronic lymphocytic leukemia: association with progression and fludarabine-refractoriness. *Blood* 118, 6904–6908, doi:10.1182/blood-2011-08-373159 (2011). [PubMed: 22039264]
13. Yoshida K et al. Frequent pathway mutations of splicing machinery in myelodysplasia. *Nature* 478, 64–69, doi:10.1038/nature10496 (2011). [PubMed: 21909114]
14. Inoue D et al. Spliceosomal disruption of the non-canonical BAF complex in cancer. *Nature* 574, 432–436, doi:10.1038/s41586-019-1646-9 (2019). [PubMed: 31597964]
15. Lee SC et al. Synthetic Lethal and Convergent Biological Effects of Cancer-Associated Spliceosomal Gene Mutations. *Cancer Cell* 34, 225–241 e228, doi:10.1016/j.ccell.2018.07.003 (2018). [PubMed: 30107174]
16. Shuai S et al. The U1 spliceosomal RNA is recurrently mutated in multiple cancers. *Nature* 574, 712–716, doi:10.1038/s41586-019-1651-z (2019). [PubMed: 31597163]
17. Karni R et al. The gene encoding the splicing factor SF2/ASF is a proto-oncogene. *Nat Struct Mol Biol* 14, 185–193, doi:10.1038/nsmb1209 (2007). [PubMed: 17310252]
18. Anczukow O et al. The splicing factor SRSF1 regulates apoptosis and proliferation to promote mammary epithelial cell transformation. *Nat Struct Mol Biol* 19, 220–228, doi:10.1038/nsmb.2207 (2012). [PubMed: 22245967]
19. Das S, Anczukow O, Akerman M & Krainer AR Oncogenic splicing factor SRSF1 is a critical transcriptional target of MYC. *Cell reports* 1, 110–117, doi:10.1016/j.celrep.2011.12.001 (2012). [PubMed: 22545246]
20. Anczukow O et al. SRSF1-Regulated Alternative Splicing in Breast Cancer. *Mol Cell* 60, 105–117, doi:10.1016/j.molcel.2015.09.005 (2015). [PubMed: 26431027]
21. Cohen-Eliav M et al. The splicing factor SRSF6 is amplified and is an oncoprotein in lung and colon cancers. *J Pathol* 229, 630–639, doi:10.1002/path.4129 (2013). [PubMed: 23132731]
22. Jensen MA, Wilkinson JE & Krainer AR Splicing factor SRSF6 promotes hyperplasia of sensitized skin. *Nat Struct Mol Biol* 21, 189–197, doi:10.1038/nsmb.2756 (2014). [PubMed: 24440982]
23. He X, Ee PL, Coon JS & Beck WT Alternative splicing of the multidrug resistance protein 1/ATP binding cassette transporter subfamily gene in ovarian cancer creates functional splice variants and is associated with increased expression of the splicing factors PTB and SRp20. *Clin Cancer Res* 10, 4652–4660, doi:10.1158/1078-0432.CCR-03-0439 (2004). [PubMed: 15269137]
24. Jia R, Li C, McCoy JP, Deng CX & Zheng ZM SRp20 is a proto-oncogene critical for cell proliferation and tumor induction and maintenance. *Int J Biol Sci* 6, 806–826, doi:10.7150/ijbs.6.806 (2010). [PubMed: 21179588]

25. Iborra S et al. Alterations in expression pattern of splicing factors in epithelial ovarian cancer and its clinical impact. *Int J Gynecol Cancer* 23, 990–996, doi:10.1097/IGC.0b013e31829783e3 (2013). [PubMed: 23748175]
26. Ghigna C et al. Cell motility is controlled by SF2/ASF through alternative splicing of the Ron protooncogene. *Mol Cell* 20, 881–890, doi:10.1016/j.molcel.2005.10.026 (2005). [PubMed: 16364913]
27. Hunger SP & Mullighan CG Acute Lymphoblastic Leukemia in Children. *N Engl J Med* 373, 1541–1552, doi:10.1056/NEJMra1400972 (2015). [PubMed: 26465987]
28. Pui CH, Relling MV & Downing JR Acute lymphoblastic leukemia. *The New England journal of medicine* 350, 1535–1548, doi:10.1056/NEJMra023001 (2004). [PubMed: 15071128]
29. Pui CH, Mullighan CG, Evans WE & Relling MV Pediatric acute lymphoblastic leukemia: where are we going and how do we get there? *Blood* 120, 1165–1174, doi:10.1182/blood-2012-05-378943 (2012). [PubMed: 22730540]
30. Pui CH & Evans WE Treatment of acute lymphoblastic leukemia. *The New England journal of medicine* 354, 166–178, doi:10.1056/NEJMra052603 (2006). [PubMed: 16407512]
31. Aifantis I, Raetz E & Buonamici S Molecular pathogenesis of T-cell leukaemia and lymphoma. *Nat Rev Immunol* 8, 380–390, doi:nri2304 [pii] 10.1038/nri2304 (2008). [PubMed: 18421304]
32. Pui CH, Robison LL & Look AT Acute lymphoblastic leukaemia. *Lancet* 371, 1030–1043, doi:10.1016/S0140-6736(08)60457-2 (2008). [PubMed: 18358930]
33. Shah A & Coleman MP Increasing incidence of childhood leukaemia: a controversy re-examined. *Br J Cancer* 97, 1009–1012, doi:10.1038/sj.bjc.6603946 (2007). [PubMed: 17712312]
34. Haydu JE & Ferrando AA Early T-cell precursor acute lymphoblastic leukaemia. *Curr Opin Hematol* 20, 369–373, doi:10.1097/MOH.0b013e3283623c61 (2013). [PubMed: 23695450]
35. Coustan-Smith E et al. Early T-cell precursor leukaemia: a subtype of very high-risk acute lymphoblastic leukaemia. *Lancet Oncol* 10, 147–156, doi:10.1016/S1470-2045(08)70314-0 (2009). [PubMed: 19147408]
36. Weng AP et al. Activating mutations of NOTCH1 in human T cell acute lymphoblastic leukemia. *Science* 306, 269–271, doi:10.1126/science.1102160 (2004). [PubMed: 15472075]
37. Real PJ et al. Gamma-secretase inhibitors reverse glucocorticoid resistance in T cell acute lymphoblastic leukemia. *Nat Med* 15, 50–58, doi:nm.1900 [pii] 10.1038/nm.1900 (2009). [PubMed: 19098907]
38. Tosello V et al. WT1 mutations in T-ALL. *Blood* 114, 1038–1045, doi:blood-2008-12-192039 [pii] 10.1182/blood-2008-12-192039 (2009). [PubMed: 19494353]
39. De Keersmaecker K & Ferrando AA TLX1-induced T-cell acute lymphoblastic leukemia. *Clin Cancer Res* 17, 6381–6386, doi:10.1158/1078-0432.CCR-10-3037 (2011). [PubMed: 21705452]
40. Zenatti PP et al. Oncogenic IL7R gain-of-function mutations in childhood T-cell acute lymphoblastic leukemia. *Nat Genet* 43, 932–939, doi:10.1038/ng.924 (2011). [PubMed: 21892159]
41. Ntziachristos P et al. Genetic inactivation of the polycomb repressive complex 2 in T cell acute lymphoblastic leukemia. *Nature medicine* 18, 298–301, doi:10.1038/nm.2651 (2012).
42. Ntziachristos P et al. Contrasting roles of histone 3 lysine 27 demethylases in acute lymphoblastic leukaemia. *Nature* 514, 513–517, doi:10.1038/nature13605 (2014). [PubMed: 25132549]
43. Trimarchi T et al. Genome-wide mapping and characterization of Notch-regulated long noncoding RNAs in acute leukemia. *Cell* 158, 593–606, doi:10.1016/j.cell.2014.05.049 (2014). [PubMed: 25083870]
44. Buonamici S et al. CCR7 signalling as an essential regulator of CNS infiltration in T-cell leukaemia. *Nature* 459, 1000–1004, doi:nature08020 [pii] 10.1038/nature08020 (2009). [PubMed: 19536265]
45. Mullighan CG & Downing JR Global genomic characterization of acute lymphoblastic leukemia. *Seminars in hematology* 46, 3–15, doi:10.1053/j.seminhematol.2008.09.005 (2009). [PubMed: 19100363]
46. Zhang J et al. The genetic basis of early T-cell precursor acute lymphoblastic leukaemia. *Nature* 481, 157–163, doi:10.1038/nature10725 (2012). [PubMed: 22237106]

47. Roberts KG & Mullighan CG Genomics in acute lymphoblastic leukaemia: insights and treatment implications. *Nat Rev Clin Oncol* 12, 344–357, doi:10.1038/nrclinonc.2015.38 (2015). [PubMed: 25781572]
48. Liu Y et al. The genomic landscape of pediatric and young adult T-lineage acute lymphoblastic leukemia. *Nature genetics* 49, 1211–1218, doi:10.1038/ng.3909 (2017). [PubMed: 28671688]
49. Robinson MD, McCarthy DJ & Smyth GK edgeR: a Bioconductor package for differential expression analysis of digital gene expression data. *Bioinformatics* 26, 139–140, doi:10.1093/bioinformatics/btp616 (2010). [PubMed: 19910308]
50. Shen S et al. rMATS: robust and flexible detection of differential alternative splicing from replicate RNA-Seq data. *Proceedings of the National Academy of Sciences of the United States of America* 111, E5593–5601, doi:10.1073/pnas.1419161111 (2014). [PubMed: 25480548]
51. Uppal S et al. The Bromodomain Protein 4 Contributes to the Regulation of Alternative Splicing. *Cell reports* 29, 2450–2460 e2455, doi:10.1016/j.celrep.2019.10.066 (2019). [PubMed: 31747612]
52. Lareau LF & Brenner SE Regulation of splicing factors by alternative splicing and NMD is conserved between kingdoms yet evolutionarily flexible. *Mol Biol Evol* 32, 1072–1079, doi:10.1093/molbev/msv002 (2015). [PubMed: 25576366]
53. Lareau LF, Inada M, Green RE, Wengrod JC & Brenner SE Unproductive splicing of SR genes associated with highly conserved and ultraconserved DNA elements. *Nature* 446, 926–929, doi:10.1038/nature05676 (2007). [PubMed: 17361132]
54. Park JW, Jung S, Rouchka EC, Tseng YT & Xing Y rMAPS: RNA map analysis and plotting server for alternative exon regulation. *Nucleic acids research* 44, W333–338, doi:10.1093/nar/gkw410 (2016). [PubMed: 27174931]
55. Tsherniak A et al. Defining a Cancer Dependency Map. *Cell* 170, 564–576 e516, doi:10.1016/j.cell.2017.06.010 (2017). [PubMed: 28753430]
56. Gerstberger S, Hafner M & Tuschl T A census of human RNA-binding proteins. *Nat Rev Genet* 15, 829–845, doi:10.1038/nrg3813 (2014). [PubMed: 25365966]
57. Lunde BM, Moore C & Varani G RNA-binding proteins: modular design for efficient function. *Nat Rev Mol Cell Biol* 8, 479–490, doi:10.1038/nrm2178 (2007). [PubMed: 17473849]
58. Wang E et al. Targeting an RNA-Binding Protein Network in Acute Myeloid Leukemia. *Cancer Cell* 35, 369–384 e367, doi:10.1016/j.ccell.2019.01.010 (2019). [PubMed: 30799057]
59. Shalem O et al. Genome-scale CRISPR-Cas9 knockout screening in human cells. *Science* 343, 84–87, doi:10.1126/science.1247005 (2014). [PubMed: 24336571]
60. Wang T et al. Gene Essentiality Profiling Reveals Gene Networks and Synthetic Lethal Interactions with Oncogenic Ras. *Cell* 168, 890–903 e815, doi:10.1016/j.cell.2017.01.013 (2017). [PubMed: 28162770]
61. Shi J et al. Discovery of cancer drug targets by CRISPR-Cas9 screening of protein domains. *Nat Biotechnol* 33, 661–667, doi:10.1038/nbt.3235 (2015). [PubMed: 25961408]
62. Hart T et al. High-Resolution CRISPR Screens Reveal Fitness Genes and Genotype-Specific Cancer Liabilities. *Cell* 163, 1515–1526, doi:10.1016/j.cell.2015.11.015 (2015). [PubMed: 26627737]
63. Neumann M et al. Mutational spectrum of adult T-ALL. *Oncotarget* 6, 2754–2766, doi:10.18632/oncotarget.2218 (2015). [PubMed: 25595890]
64. Puente XS et al. Whole-genome sequencing identifies recurrent mutations in chronic lymphocytic leukaemia. *Nature* 475, 101–105, doi:10.1038/nature10113 (2011). [PubMed: 21642962]
65. Malcovati L et al. Clinical significance of SF3B1 mutations in myelodysplastic syndromes and myelodysplastic/myeloproliferative neoplasms. *Blood* 118, 6239–6246, doi:10.1182/blood-2011-09-377275 (2011). [PubMed: 21998214]
66. Van Vlierberghe P et al. ETV6 mutations in early immature human T cell leukemias. *J Exp Med* 208, 2571–2579, doi:10.1084/jem.20112239 (2011). [PubMed: 22162831]
67. Koh CM et al. MYC regulates the core pre-mRNA splicing machinery as an essential step in lymphomagenesis. *Nature* 523, 96–100, doi:10.1038/nature14351 (2015). [PubMed: 25970242]
68. Hsu TY et al. The spliceosome is a therapeutic vulnerability in MYC-driven cancer. *Nature* 525, 384–388, doi:10.1038/nature14985 (2015). [PubMed: 26331541]

69. Su H et al. SHQ1 regulation of RNA splicing is required for T-lymphoblastic leukemia cell survival. *Nat Commun* 9, 4281, doi:10.1038/s41467-018-06523-4 (2018). [PubMed: 30323192]
70. Jin Q et al. USP7 Cooperates with NOTCH1 to Drive the Oncogenic Transcriptional Program in T-Cell Leukemia. *Clin Cancer Res* 25, 222–239, doi:10.1158/1078-0432.CCR-18-1740 (2019). [PubMed: 30224337]
71. Rawat R, Starczynowski DT & Ntziachristos P Nuclear deubiquitination in the spotlight: the multifaceted nature of USP7 biology in disease. *Curr Opin Cell Biol* 58, 85–94, doi:10.1016/j.ceb.2019.02.008 (2019). [PubMed: 30897496]
72. Kumar D et al. Degradation of splicing factor SRSF3 contributes to progressive liver disease. *J Clin Invest* 130, 4477–4491, doi:10.1172/JCI127374 (2019).
73. Jayabalan AK et al. NEDDylation promotes stress granule assembly. *Nat Commun* 7, 12125, doi:10.1038/ncomms12125 (2016). [PubMed: 27381497]
74. Maertens GN, El Messaoudi-Aubert S, Elderkin S, Hiom K & Peters G Ubiquitin-specific proteases 7 and 11 modulate Polycomb regulation of the INK4a tumour suppressor. *EMBO J* 29, 2553–2565, doi:10.1038/emboj.2010.129 (2010). [PubMed: 20601937]
75. Georges A, Marcon E, Greenblatt J & Frappier L Identification and Characterization of USP7 Targets in Cancer Cells. *Sci Rep* 8, 15833, doi:10.1038/s41598-018-34197-x (2018). [PubMed: 30367141]
76. Sowa ME, Bennett EJ, Gygi SP & Harper JW Defining the human deubiquitinating enzyme interaction landscape. *Cell* 138, 389–403, doi:10.1016/j.cell.2009.04.042 (2009). [PubMed: 19615732]
77. Palazon-Riquelme P et al. USP7 and USP47 deubiquitinases regulate NLRP3 inflammasome activation. *EMBO Rep* 19, e44766, doi:10.15252/embr.201744766 (2018). [PubMed: 30206189]
78. Chauhan D et al. A small molecule inhibitor of ubiquitin-specific protease-7 induces apoptosis in multiple myeloma cells and overcomes bortezomib resistance. *Cancer Cell* 22, 345–358, doi:10.1016/j.ccr.2012.08.007 (2012). [PubMed: 22975377]
79. Altun M et al. Activity-based chemical proteomics accelerates inhibitor development for deubiquitylating enzymes. *Chem Biol* 18, 1401–1412, doi:10.1016/j.chembiol.2011.08.018 (2011). [PubMed: 22118674]
80. Tzelepis K et al. SRPK1 maintains acute myeloid leukemia through effects on isoform usage of epigenetic regulators including BRD4. *Nat Commun* 9, 5378, doi:10.1038/s41467-018-07620-0 (2018). [PubMed: 30568163]
81. Seiler M et al. H3B-8800, an orally available small-molecule splicing modulator, induces lethality in spliceosome-mutant cancers. *Nature medicine* 24, 497–504, doi:10.1038/nm.4493 (2018).
82. Aird D et al. Sensitivity to splicing modulation of BCL2 family genes defines cancer therapeutic strategies for splicing modulators. *Nat Commun* 10, 137, doi:10.1038/s41467-018-08150-5 (2019). [PubMed: 30635584]
83. Hirano Y et al. A heterodimeric complex that promotes the assembly of mammalian 20S proteasomes. *Nature* 437, 1381–1385, doi:10.1038/nature04106 (2005). [PubMed: 16251969]
84. Sasaki K et al. PAC1 gene knockout reveals an essential role of chaperone-mediated 20S proteasome biogenesis and latent 20S proteasomes in cellular homeostasis. *Molecular and cellular biology* 30, 3864–3874, doi:10.1128/MCB.00216-10 (2010). [PubMed: 20498273]
85. Wani PS, Rowland MA, Ondracek A, Deeds EJ & Roelofs J Maturation of the proteasome core particle induces an affinity switch that controls regulatory particle association. *Nat Commun* 6, 6384, doi:10.1038/ncomms7384 (2015). [PubMed: 25812915]
86. Trapnell C et al. Transcript assembly and quantification by RNA-Seq reveals unannotated transcripts and isoform switching during cell differentiation. *Nat Biotechnol* 28, 511–515, doi:nbt.1621 [pii] 10.1038/nbt.1621 (2010). [PubMed: 20436464]
87. Anders S, Reyes A & Huber W Detecting differential usage of exons from RNA-seq data. *Genome Res* 22, 2008–2017, doi:10.1101/gr.133744.111 (2012). [PubMed: 22722343]
88. Koyama D et al. Proteasome inhibitors exert cytotoxicity and increase chemosensitivity via transcriptional repression of Notch1 in T-cell acute lymphoblastic leukemia. *Leukemia* 28, 1216–1226, doi:10.1038/leu.2013.366 (2014). [PubMed: 24301524]

89. Takahashi K et al. Anti-leukemic activity of bortezomib and carfilzomib on B-cell precursor ALL cell lines. *PLoS one* 12, e0188680, doi:10.1371/journal.pone.0188680 (2017). [PubMed: 29236701]
90. Boccadoro M, Morgan G & Cavenagh J Preclinical evaluation of the proteasome inhibitor bortezomib in cancer therapy. *Cancer Cell Int* 5, 18, doi:10.1186/1475-2867-5-18 (2005). [PubMed: 15929791]
91. Satou Y et al. Proteasome inhibitor, bortezomib, potently inhibits the growth of adult T-cell leukemia cells both in vivo and in vitro. *Leukemia* 18, 1357–1363, doi:10.1038/sj.leu.2403400 (2004). [PubMed: 15190257]
92. Foucquier J & Guedj M Analysis of drug combinations: current methodological landscape. *Pharmacol Res Perspect* 3, e00149, doi:10.1002/prp2.149 (2015). [PubMed: 26171228]
93. Black KL et al. Aberrant splicing in B-cell acute lymphoblastic leukemia. *Nucleic Acids Res* 46, 11357–11369, doi:10.1093/nar/gky946 (2018). [PubMed: 30357359]
94. Kahles A et al. Comprehensive Analysis of Alternative Splicing Across Tumors from 8,705 Patients. *Cancer Cell* 34, 211–224 e216, doi:10.1016/j.ccell.2018.07.001 (2018). [PubMed: 30078747]
95. Aubol BE et al. Processive phosphorylation of alternative splicing factor/splicing factor 2. *Proceedings of the National Academy of Sciences of the United States of America* 100, 12601–12606, doi:10.1073/pnas.1635129100 (2003). [PubMed: 14555757]
96. Braun CJ et al. Coordinated Splicing of Regulatory Detained Introns within Oncogenic Transcripts Creates an Exploitable Vulnerability in Malignant Glioma. *Cancer Cell* 32, 411–426 e411, doi:10.1016/j.ccell.2017.08.018 (2017). [PubMed: 28966034]
97. Bezzi M et al. Regulation of constitutive and alternative splicing by PRMT5 reveals a role for Mdm4 pre-mRNA in sensing defects in the spliceosomal machinery. *Genes & development* 27, 1903–1916, doi:10.1101/gad.219899.113 (2013). [PubMed: 24013503]
98. Fong JY et al. Therapeutic Targeting of RNA Splicing Catalysis through Inhibition of Protein Arginine Methylation. *Cancer Cell* 36, 194–209 e199, doi:10.1016/j.ccell.2019.07.003 (2019). [PubMed: 31408619]
99. Stamm S Regulation of alternative splicing by reversible protein phosphorylation. *J Biol Chem* 283, 1223–1227, doi:10.1074/jbc.R700034200 (2008). [PubMed: 18024427]
100. Zhang L et al. Cross-talk between PRMT1-mediated methylation and ubiquitylation on RBM15 controls RNA splicing. *Elife* 4:e07938 doi:10.7554/eLife.07938 (2015). [PubMed: 26575292]
101. Moulton VR, Gillooly AR & Tsokos GC Ubiquitination regulates expression of the serine/arginine-rich splicing factor 1 (SRSF1) in normal and systemic lupus erythematosus (SLE) T cells. *J Biol Chem* VOL.289, NO.7, 4126–4134, doi:10.1074/jbc.M113.518662 (2014). [PubMed: 24368769]
102. Bellare P et al. A role for ubiquitin in the spliceosome assembly pathway. *Nat Struct Mol Biol* 15, 444–451, doi:10.1038/nsmb.1401 (2008). [PubMed: 18425143]
103. Bellare P, Kutach AK, Rines AK, Guthrie C & Sontheimer EJ Ubiquitin binding by a variant Jab1/MPN domain in the essential pre-mRNA splicing factor Prp8p. *RNA* 12, 292–302, doi:10.1261/rna.2152306 (2006). [PubMed: 16428608]
104. Fang J et al. Ubiquitination of hnRNPA1 by TRAF6 links chronic innate immune signaling with myelodysplasia. *Nat Immunol* 18, 236–245, doi:10.1038/ni.3654 (2017). [PubMed: 28024152]
105. Paoletta BR et al. Copy-number and gene dependency analysis reveals partial copy loss of wild-type SF3B1 as a novel cancer vulnerability. *Elife* 6: e23268 doi:10.7554/eLife.23268 (2017). [PubMed: 28177281]
106. Steensma DP, et al., Results of a Clinical Trial of H3B-8800, a Splicing Modulator, in Patients with Myelodysplastic Syndromes (MDS), Acute Myeloid Leukemia (AML) or Chronic Myelomonocytic Leukemia (CMML). The American Society of Hematology, 61st Annual Meeting and Exposition (2019), 134 (Supplement\_1): 673.
107. Yatim A et al. NOTCH1 nuclear interactome reveals key regulators of its transcriptional activity and oncogenic function. *Mol Cell* 48, 445–458, doi:10.1016/j.molcel.2012.08.022 (2012). [PubMed: 23022380]

108. Kourtis N et al. Oncogenic hijacking of the stress response machinery in T cell acute lymphoblastic leukemia. *Nature medicine* 24, 1157–1166, doi:10.1038/s41591-018-0105-8 (2018).
109. Milani G et al. Low PKC $\alpha$  expression within the MRD-HR stratum defines a new subgroup of childhood T-ALL with very poor outcome. *Oncotarget* 5, 5234–5245, doi:10.18632/oncotarget.2062 (2014). [PubMed: 25026300]
110. Serafin V et al. Phosphoproteomic analysis reveals hyperactivation of mTOR/STAT3 and LCK/Calcineurin axes in pediatric early T-cell precursor ALL. *Leukemia* 31, 1007–1011, doi:10.1038/leu.2017.13 (2017). [PubMed: 28082737]
111. Subramanian A et al. Gene set enrichment analysis: a knowledge-based approach for interpreting genome-wide expression profiles. *Proc Natl Acad Sci U S A* 102, 15545–15550, doi:10.1073/pnas.0506580102 (2005). [PubMed: 16199517]
112. Chen EY et al. Enrichr: interactive and collaborative HTML5 gene list enrichment analysis tool. *BMC Bioinformatics* 14, 128, doi:10.1186/1471-2105-14-128 (2013). [PubMed: 23586463]
113. Meyers RM et al. Computational correction of copy number effect improves specificity of CRISPR-Cas9 essentiality screens in cancer cells. *Nature genetics* 49, 1779–1784, doi:10.1038/ng.3984 (2017). [PubMed: 29083409]
114. Ntziachristos P et al. Contrasting roles of histone 3 lysine 27 demethylases in acute lymphoblastic leukaemia. *Nature* 514, 513–517, doi:10.1038/nature13605 (2014). [PubMed: 25132549]
115. Ianevski A, He L, Aittokallio T & Tang J SynergyFinder: a web application for analyzing drug combination dose-response matrix data. *Bioinformatics* 33, 2413–2415, doi:10.1093/bioinformatics/btx162 (2017). [PubMed: 28379339]
116. Farid R, Day T, Friesner RA & Pearlstein RA New insights about HERG blockade obtained from protein modeling, potential energy mapping, and docking studies. *Bioorg Med Chem* 14, 3160–3173, doi:10.1016/j.bmc.2005.12.032 (2006). [PubMed: 16413785]
117. Bhachoo J & Beuming T Investigating Protein-Peptide Interactions Using the Schrodinger Computational Suite. *Methods Mol Biol* 1561, 235–254, doi:10.1007/978-1-4939-6798-8\_14 (2017). [PubMed: 28236242]
118. Chen VB et al. MolProbity: all-atom structure validation for macromolecular crystallography. *Acta Crystallogr D Biol Crystallogr* 66, 12–21, doi:10.1107/S09074444909042073 (2010). [PubMed: 20057044]

**STATEMENT OF SIGNIFICANCE**

Our study provides a new proof-of-principle for posttranslational regulation of splicing factors independently of mutations in the aggressive T-cell leukemia. It further suggests a new drug combination of splicing and proteasomal inhibitors, a concept that might apply to other diseases with or without mutations affecting the splicing machinery.

Author Manuscript

Author Manuscript

Author Manuscript

Author Manuscript

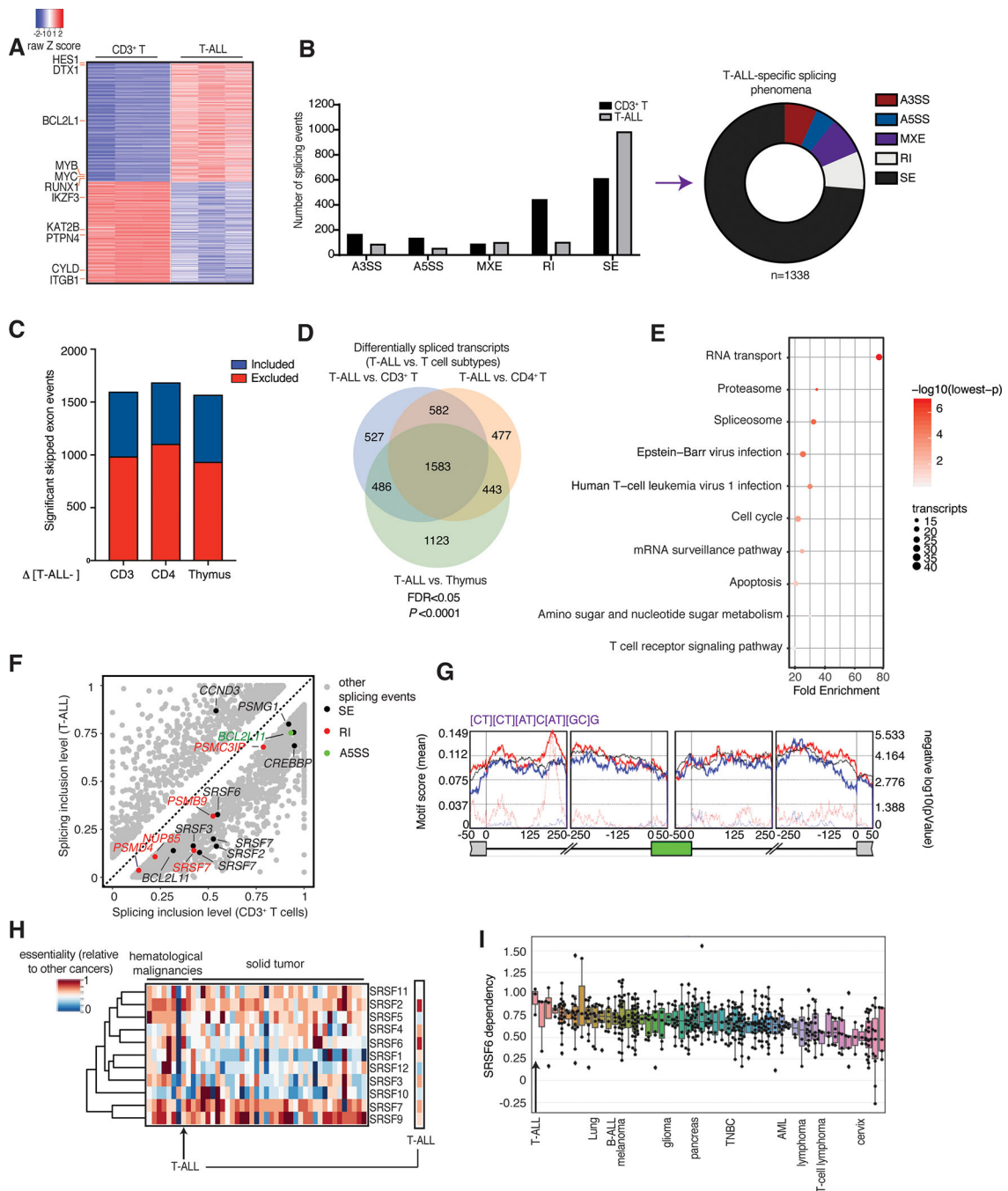


**Fig. 1. Extensive changes in exon skipping phenomena in T-ALL compared to physiological T cells.**

**A**, Heatmap of gene expression changes representing 630 significantly up-regulated genes and 531 down-regulated genes in T-ALL patient samples compared to CD3<sup>+</sup> T cells, ranked based on expression level in T-ALL ( $n=3$ , adj.  $P<0.01$ ). **B**, Differential splicing in T-ALL versus CD3<sup>+</sup> T cells. Bar graph (left) represents different types of splicing events; pie chart (right) shows T-ALL specific splicing phenomena (correspond to the grey bars). The plot represents the MATS analysis using three biological replicates per group. Only events that



passed the statistics threshold (FDR, false discovery rate  $<0.05$ ) and percent spliced in (PSI)  $> 0.1$  (10% of the transcripts of a given gene) are taken into consideration. Exon skipping (SE) is the type of event affected most significantly. A3SS, alternative 3' splice sites; A5SS, alternative 5' splice sites; MXE, mutually exclusive exons; RI, intron retention. **C**, Directionality of exon skipping in T-ALL compared to T-cell subtypes, where positive (blue) and negative (red) values represent exon inclusion and exclusion, respectively. Please note there is a higher number of skipped exons in T-ALL (red) compared to any T cell subtype. Panels **B** and **C** collectively show that there are more skipped exons in T-ALL compared to normal T cells. **D**, Overlapping transcripts affected by splicing changes in T-ALL compared to CD3<sup>+</sup> T cells, CD4<sup>+</sup> T cells, and thymocytes ( $FDR < 0.05$ ). **E**, Kyoto Encyclopedia of Genes and Genomes (KEGG) analysis showing main transcript pathways enriched in splicing events in T-ALL compared to CD3<sup>+</sup> T cells. Transcript categories are ranked based on the enrichment score,  $P$  value and size of the group. **F**, Scatterplot of splicing changes and distribution in T-ALL compared to CD3<sup>+</sup> T cells. Selected transcripts are colored based on the type of differentially spliced event. Transcripts presenting PSI $>0.1$  are shown. **G**, *De novo* binding motif discovery based on exon skipping data (including the skipped exon and flanking intron/exon sequences) in T-ALL vs. CD3<sup>+</sup> T cells using rMAPS. SRSF6-bound motif enrichment in skipped exons in T-ALL (red) and in included exons in CD3<sup>+</sup> T-cells (in blue) is shown. Background motif enrichment is shown in black and  $-\log(p \text{ Value})$  over the background is represented by red and blue dotted lines. **H**, Relative essentiality of the SRSF gene family across different types of cancer cell lines. Essentiality data, reflecting the importance of individual genes for cellular fitness, was obtained from the Project *Achilles* CRISPR-Cas9 screening dataset of 563 cancer cell lines. **I**, Essentiality for SRSF6 amongst different cancer types from the Project *Achilles*. A gene essentiality score of 1 is typical for genes considered pan-essential, such as ribosome components. T-ALL and other representative cancer types are shown. B-ALL, B cell acute lymphoblastic leukemia; TNBC, triple-negative breast cancer; AML, acute myeloid leukemia.

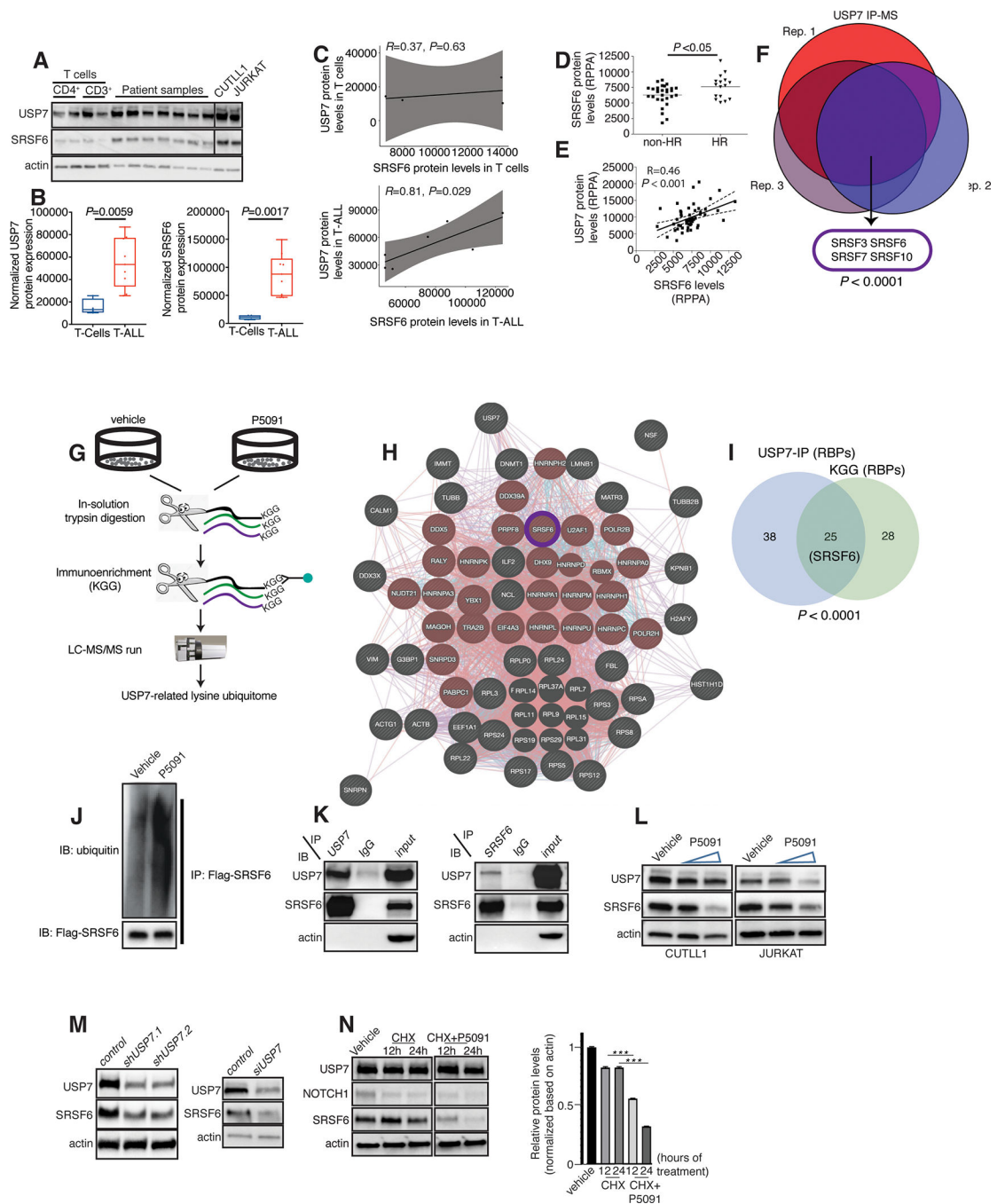


**Fig. 2. Posttranslational regulation of SRSF6 by USP7.**

**A**, Immunoblot showing SRSF6 protein levels in normal CD4<sup>+</sup> T-cells ( $n=2$ ) and CD3<sup>+</sup> T cells ( $n=2$ ), T-ALL patients ( $n=7$ ), and CUTLL1 and JURKAT cells. **B**, **C**, Quantification of immunoblot bands presented in **A**. USP7 and SRSF6 protein levels are higher in T-ALL compared to T cells (**B**). USP7 protein levels significantly correlate with SRSF6 levels in T-ALL (**C**). Actin is used as a loading control. **D**, **E**, RPPA analysis for SRSF6 protein levels in HR ( $n=16$ ) vs. non-HR T-ALL ( $n=31$ ) cases (**D**) and correlation with USP7 expression (**E**). **F**, USP7 immunoprecipitation coupled to mass spectrometry (IP-MS) analysis in

JURKAT cells. Shown is the overlap of USP7-associated proteins across 3 biological replicates, revealing splicing factors associated with USP7. **G**, Schematic representation of the USP7-related lysine ubiquitome analysis in JURKAT cells. **H**, Network analysis of the overlapped proteins of USP7 immunoprecipitation-mass spectrometry and KGG mass spectrometry using GeneMANIA. Splicing related proteins are highlighted in red. **I**, Analysis of the overlapping data sets for USP7 immunoprecipitation-mass spectrometry and KGG mass spectrometry studies reveals a significant number of RNA binding proteins in common (25,  $P < 0.0001$ ). **J**, Immunoblot for detection of ubiquitination upon lentiviral expression of Flag-tagged SRSF6 in CUTLL1 cells coupled to treatment with P5091. The Flag epitope was used for SRSF6 pull-down. A representative blot for one biological replicate of vehicle- and P5091-treated CUTLL1 cells for the pull-down is shown. **K**, Immunoblots (WB) following immunoprecipitation (IP) of USP7 (left panel) and SRSF6 (right panel) in JURKAT cells, showing interaction of USP7 and SRSF6. **L**, Immunoblot studies for USP7 and SRSF6 using CUTLL1 and JURKAT cells upon treatment with increasing concentrations of P5091. Actin is used as a loading control. **M**, Immunoblot studies for USP7 and SRSF6 upon silencing of *USP7* using two different short-hairpin RNAs in CUTLL1 cells (left panel) or siRNA over a period of 96h in 293T cells (right panel). Actin is used as a loading control. **N**, Immunoblot analysis for SRSF6 levels upon treatment with cycloheximide (CHX, 200 $\mu$ g/ml), or combination of CHX with P5091 (10 $\mu$ M) over a period of 24h. Representative blot from one out of three experiments (left) and quantification of protein levels from three experiments (right) are shown (\*\*\*,  $P < 0.001$ ).

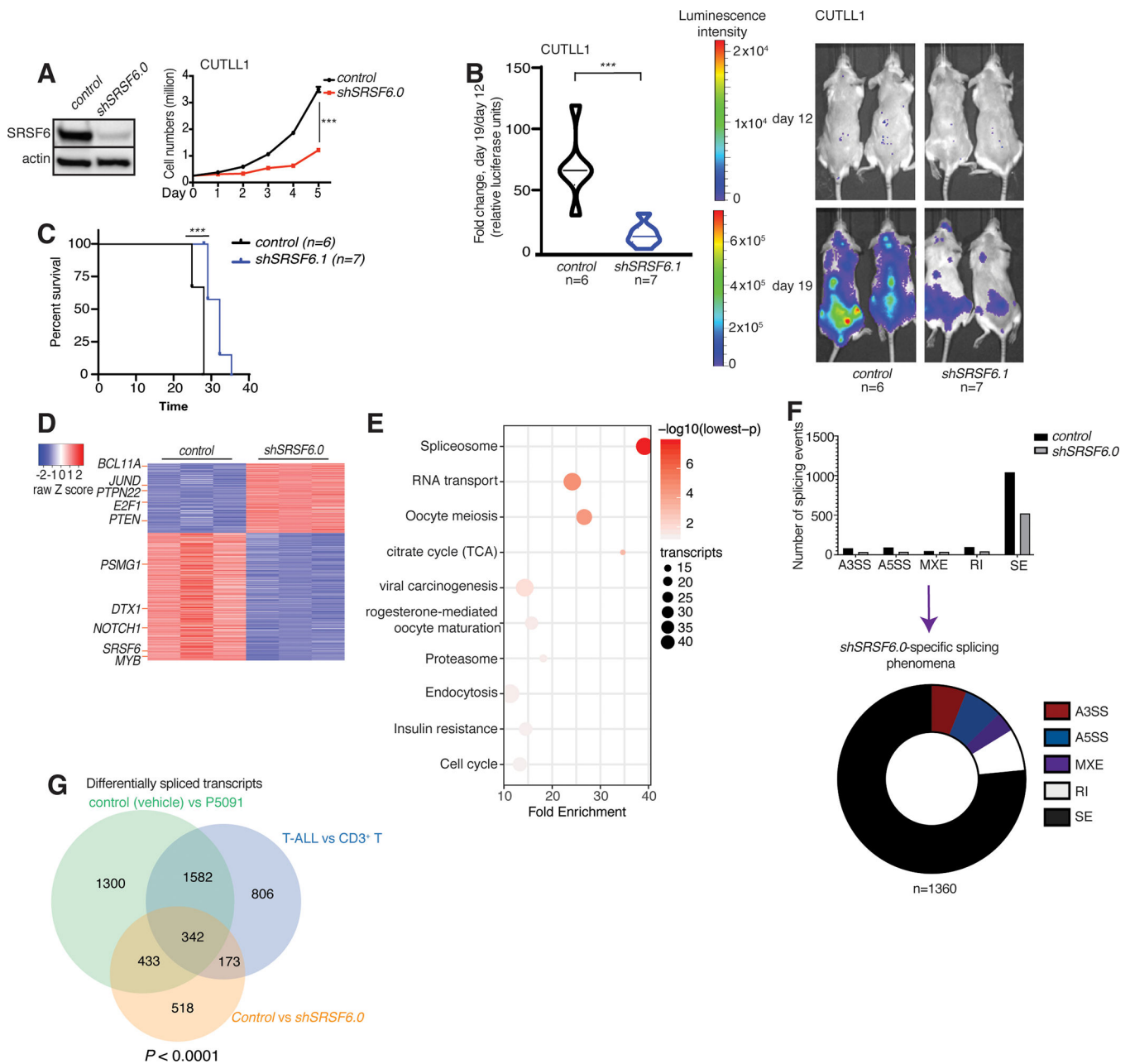


**Fig. 3. SRSF6 silencing inhibits T-ALL growth.**

**A**, Immunoblot analysis of SRSF6 protein levels (left) as well as growth of control- and *shSRSF6*-expressing CUTLL1 cells over a period of 5 days ( $n=3$ , right panel, \*\*\*  $P < 0.001$ ). Actin is used as loading control. **B**, Luciferase-expressing CUTLL1 cells were transduced with lentiviral vector expressing a control hairpin RNA or *shSRSF6.1*, selected using puromycin for a period of 7 days, and injected intravenously into immunocompromised mice. Leukemic burden was assessed via blast detection in mouse body using bioluminescence and IVIS equipment twice per week. Relative bioluminescence intensity is shown for two representative mouse per treatment group on days 12 and 19 of treatment (right panel). The fold change in total flux from day 12 to day 19 is shown on the left

(control, n=6; *shSRSF6.1*, n=7, \*\*\*  $P<0.001$ ). **C**, Survival analysis of mice transplanted with control hairpin RNA or *shSRSF6.1*-expressing CUTLL1 cells (control, n=6; *shSRSF6.1*, n=7, \*\*\*  $P<0.001$ ). **D**, Heatmap of changes in gene expression representing 543 significantly up-regulated genes and 1001 down-regulated genes in *shSRSF6.0*-expressing compared to control JURKAT cells (adj.  $P<0.01$ ). **E**, Kyoto Encyclopedia of Genes and Genomes (KEGG) analysis showing main transcript pathways enriched for gene expression changes in *shSRSF6.0*-expressing JURKAT cells compared to the control JURKAT population. **F**, Splicing analysis in the *shSRSF6.0* sample and comparison to control JURKAT cells. Bar graph (top) represents different types of splicing events in each genotype, pie chart (bottom) shows *shSRSF6.0*-specific splicing phenomena. Skipped exons (SE) is the main event category. The plot represents the MATS analysis using three biological replicates per group. Only events that passed the statistics threshold ( $FDR<0.05$ ) and present with  $PSI>0.1$  are presented. **G**, Overlap of transcripts presenting with splicing changes in DMSO (vehicle) vs. P5091, CD3<sup>+</sup> T cells vs. T-ALL cells, as well as control vs. *shSRSF6.0* conditions. Analysis shows 342 genes common in all comparisons ( $P<0.0001$ ).

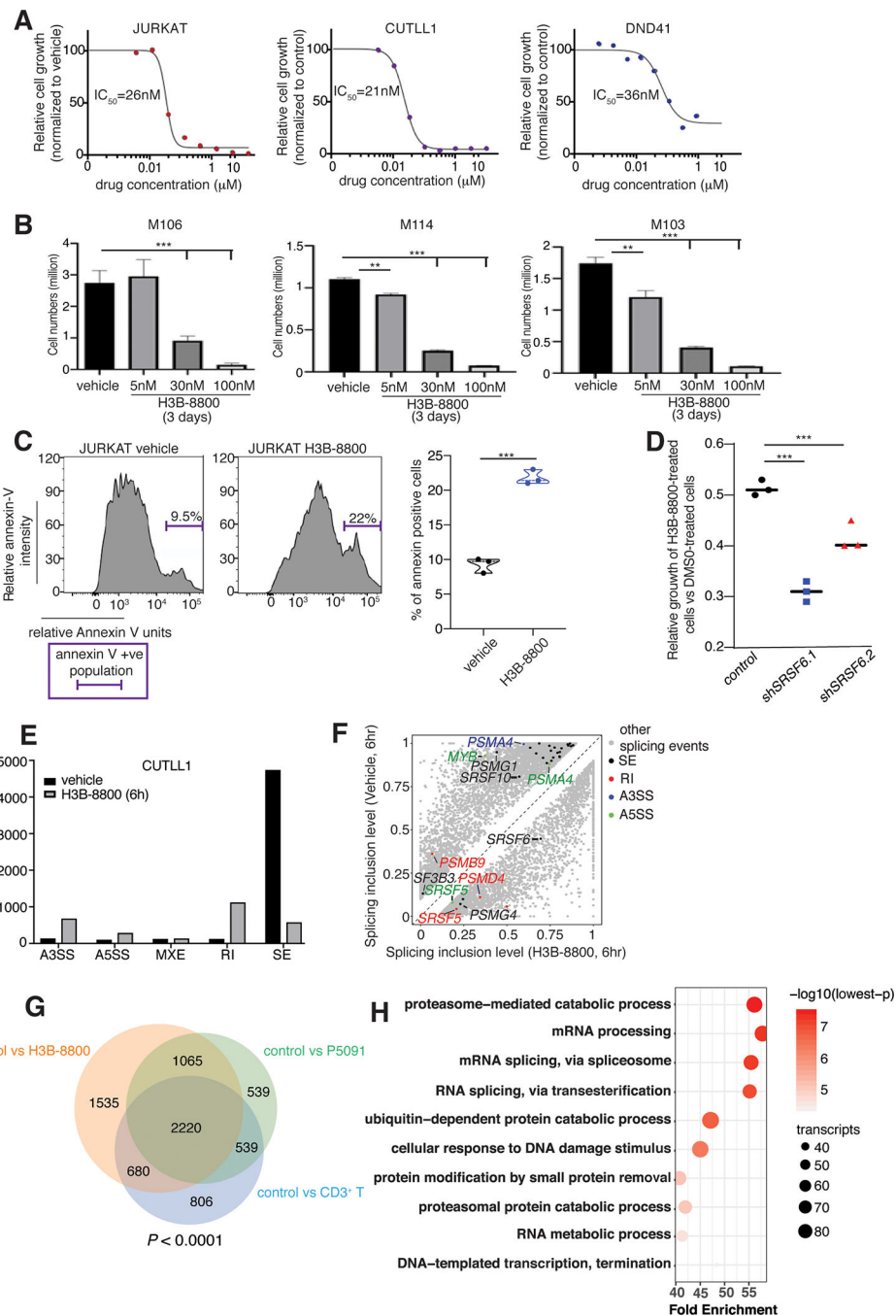


**Fig. 4. Inhibition of splicing blocks the growth of T-cell leukemia tumors.**

**A**, IC<sub>50</sub> curves of splicing inhibition using H3B-8800 in T-ALL cell lines (JURKAT, CUTLL1, DND41) over a period of 72h. To study cell growth, 3,000 cells per well were used and incubated with alamarBlue for 4 h. **B**, Cell numbers for three patient samples treated with vehicle and increasing concentrations of H3B-800 up to 100nM over a 72h period. Live human T-cell leukemia cell populations were measured using cytometry and staining with hCD7 and hCD45 antibodies (\*\*\*,  $P < 0.001$ ). **C**, Annexin V staining plots (left panel) and quantification (right panel) upon treatment with 30 nM H3B-8800 over a

period of 48 h in JURKAT T-ALL cells (n=3, \*\*\*,  $P<0.001$ ). **D**, Relative growth of H3B-8800-treated cells compared to vehicle-treated cells is shown for *control*, *shSRSF6.1*, and *shSRSF6.2*-expressing CUTLL1 cell populations. *shSRSF6.1*-expressing cells present with an increased sensitivity to splicing inhibition compared to control cells (n=3, \*\*\*,  $P<0.001$ ). **E**, Number of splicing events in CUTLL1 cells upon treatment with H3B-8800 for 6 h versus DMSO (vehicle). Retained introns (RI) and skipped exons (SE) were the two event categories affected most dramatically. The plot represents the MATS analysis using three biological replicates per group. Only events that passed the statistics threshold (FDR  $<0.05$ ) and percent spliced in (PSI)  $>0.1$  are presented. **F**, Scatterplot of splicing changes and distribution in H3B-8800-treated CUTLL1 cells (6h) compared to vehicle-treated CUTLL1 cells. Selected transcripts are colored by the type of differentially spliced event. Splicing is quantified using a “percent spliced in” value (PSI, or  $\psi$  value) and changes affecting at least 10% of transcripts are presented. **G**, Overlapping of transcripts affected by splicing changes in vehicle-treated JURKAT cells in comparison to H3B-8800- and P5091-treated JURKAT cells as well as CD3<sup>+</sup> T cells. Analysis identified 2220 transcripts alternatively spliced in vehicle-treated JURKAT cells compared to the three other conditions. **H**, Gene ontology analysis of 2220 overlapping genes from (**G**) showing enrichment of critical transcript families, including the proteasome- and spliceosome machinery-encoding transcripts.

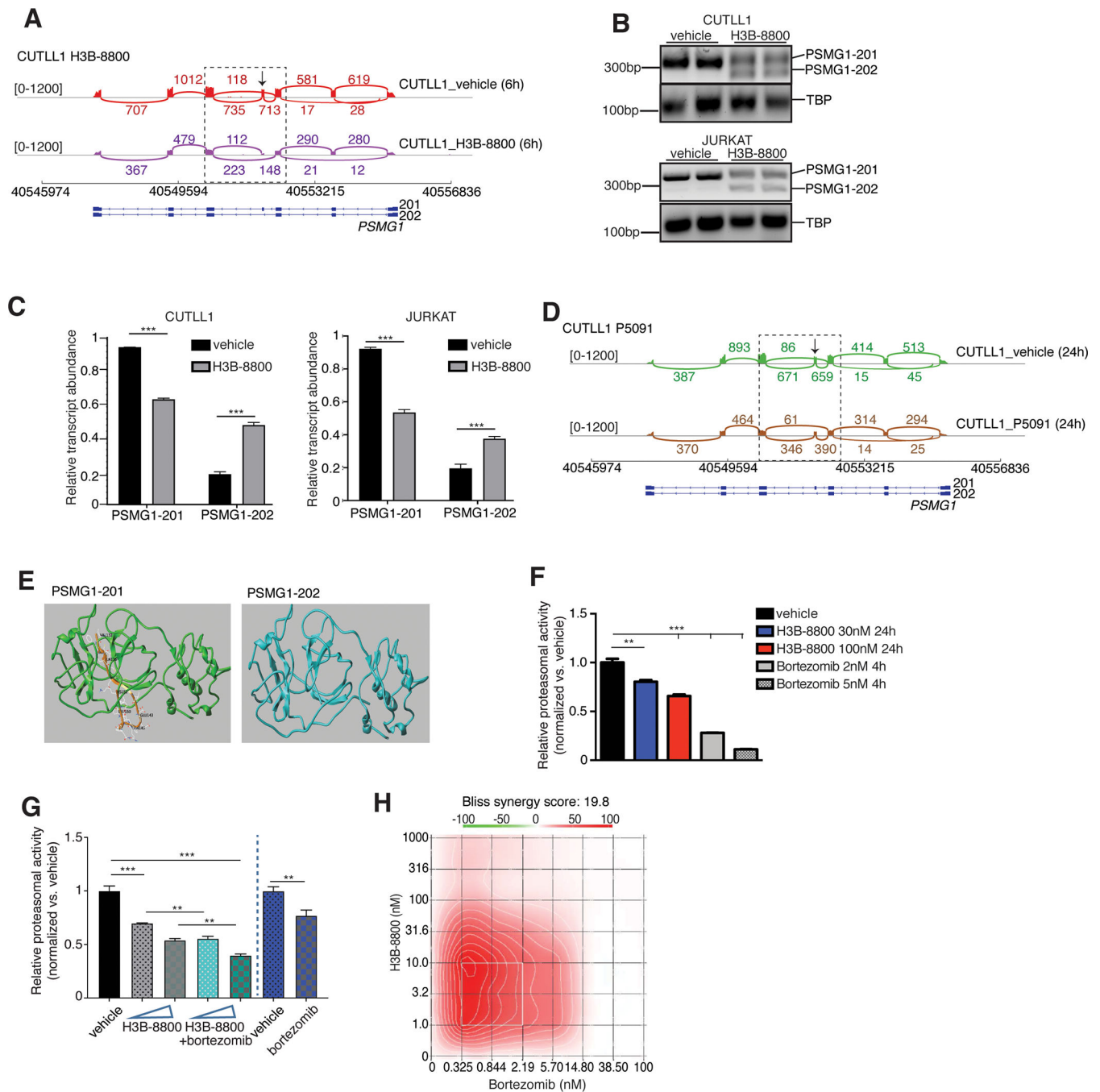


**Fig. 5. Extensive splicing changes affecting proteasome subunits is a vulnerability in T-cell leukemia.**

**A**, Sashimi plots representing splicing and exon-exon junctions for the *PSMG1* transcript in CUTLL1 cells treated with 30nM H3B-8800 for 6 h. DNA/gene is shown along the horizontal axis. Thicker sections represent exons coding for protein sequence. Numbers over the lines connecting exons represent the number of reads mapped to that exon-exon junction. **B**, PCR-based analysis coupled to electrophoresis for detection of PSMG1–201 and PSMG1–202 isoforms upon H3B-8800 treatment (30nM, 6h) using CUTLL1 (top panel) and



JURKAT cells (bottom panel). **C**, Quantification of band intensities presented in **B**. \* \* \*  $P < 0.001$ . **D**, Sashimi plots representing splicing and exon-exon junctions for the *PSMG1* transcript in CUTLL1 cells treated with 10 $\mu$ M P5091 for 24 h. RNA sequence is shown along the horizontal axis. Thicker sections represent exons coding for protein sequence. Numbers over the lines connecting exons represent the number of reads mapped to that junction. **E**, Modeling of PSMG1 protein structure changes upon H3B-8800 treatment. Structures of constructs 201 and 202 (consensus coding sequence (CCDS) CCDS13660 and CCDS13661 correspondingly for protein Q95456) were displayed. Brown and yellow part represents 21 amino acids present in 201 but missing from 202. Amino acids VAL123, GLN136, GLU143, GLN145, LEU150 and CYS152 are highlighted. **F**, Measurement of proteasome activity using a luminescence-based method upon treatment of JURKAT cells with 30nM and 100nM H3B-8800 for 24h. Bortezomib was used as a positive control for proteasome inhibition (\*\*,  $P < 0.01$ , \*\*\*,  $P < 0.001$ ). **G**, Measurement of proteasome activity using a luminescence-based method upon treatment of JURKAT cells with 30nM and 100nM H3B-8800 for 24h, alone (grey bars) or in combination with 0.5nM bortezomib (4h treatment, green bars). Bortezomib was used as a positive control for proteasome inhibition (0.5nM, 4h treatment, blue bar, \*\*,  $P < 0.01$ , \*\*\*,  $P < 0.001$ ). **H**, Synergy heatmaps for proteasomal inhibitor bortezomib and H3B-8800 treatment over a period of 3 days in JURKAT cells. Bliss analysis is shown. This result indicates synergy at the lower dose range for both drugs which might allow for combinatorial drug treatment with minimum toxicity.

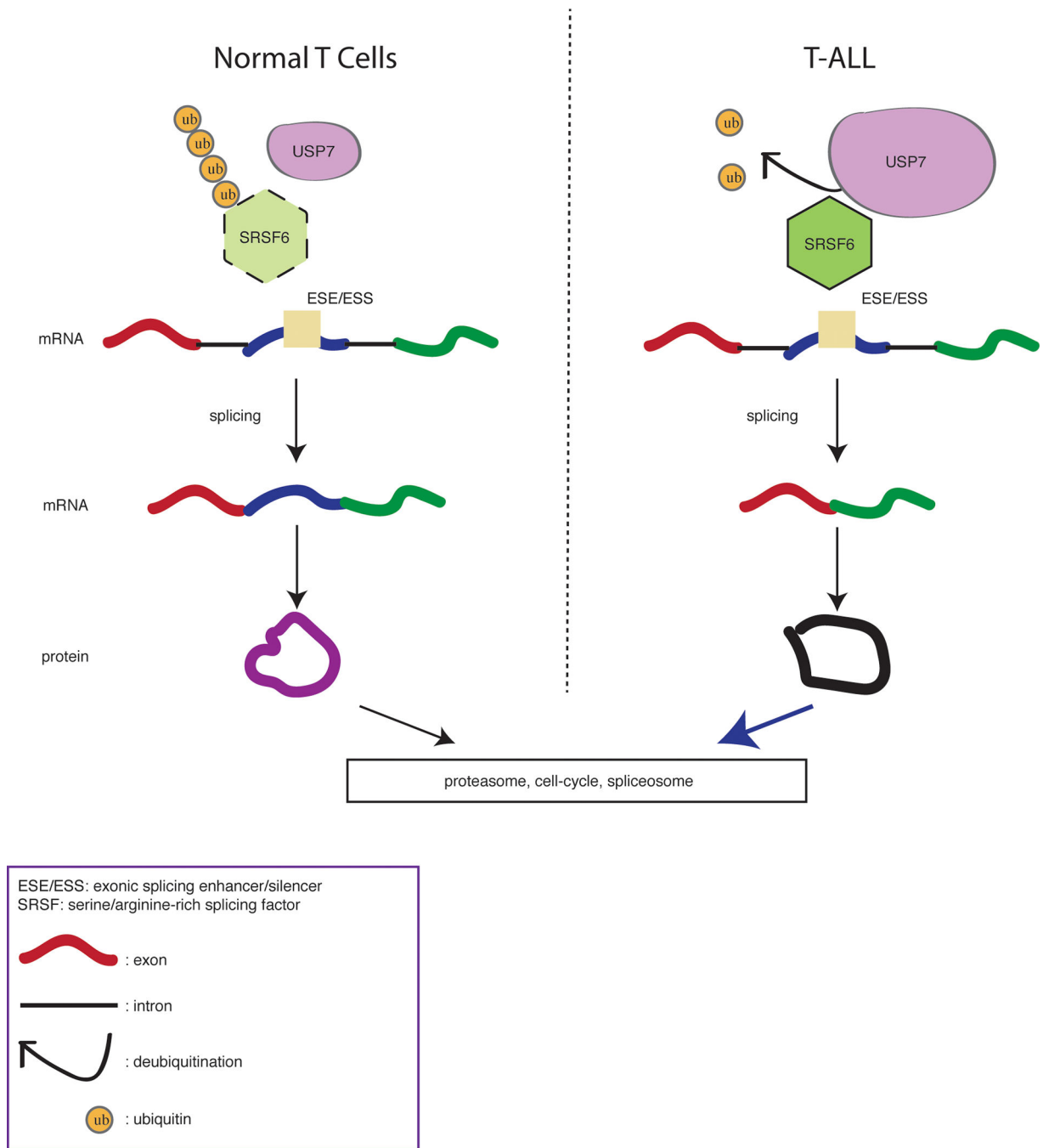


**Fig. 6. Schematic representation of abnormal splicing via deubiquitination in T-cell leukemia.** T cells exhibit physiological levels of USP7 and SRSF6 coupled to normal splicing. Aberrantly high levels of USP7 (illustrated by the larger size of USP7 scheme in the right panel) contribute to high levels of SRSF6 and exon skipping changes in leukemia.